11

CO_2 Emissions Targeting for Petroleum Refinery Optimization

Mohmmad A. Al-Mayyahi[1], Andrew F.A. Hoadley[1] and Gade Pandu Rangaiah[2]
[1]Department of Chemical Engineering, Monash University, Australia
[2]Department of Chemical and Biomolecular Engineering,
National University of Singapore, Singapore

11.1 Introduction

Petroleum refineries are under increasing pressure to minimize emissions of greenhouse gases, mainly CO_2, to comply with the environmental regulations such as the Kyoto protocol by the United Nations Framework Convention and Climate Change (UNFCC). Because of this trend, there is considerable interest from the petroleum-refining industry to target and minimize CO_2 emissions from different refinery processes. Many studies have been published recently on the CO_2 emissions produced in petroleum refining. These can be categorized as either academic or technical.

In the academic studies, different methodologies are used to allocate / target and minimize CO_2 emissions. The allocation of refinery CO_2 emissions was investigated using refinery LP models and single-objective optimization [1–5]. These studies quantified and compared CO_2 emissions due to production of different finished products such as gasoline and diesel. However, the calculations were based on simple linear relations between product demand/specifications and operating conditions. Moreover, the value of the results strongly depends on the structure of the refinery concerned and the cost assigned for CO_2 emissions. Szklo and Schaeffer [6] investigated the impact of the more restrictive environmental quality of petroleum products on the energy consumption and consequential CO_2 emissions in the refinery. They also reviewed many energy-saving strategies in refineries such as

Multi-Objective Optimization in Chemical Engineering: Developments and Applications, First Edition.
Edited by Gade Pandu Rangaiah and Adrián Bonilla-Petriciolet.

improvement of heat integration and alternative treatment processes. Ba-Shammakh [7] developed a general mathematical model for an oil refinery. Single-objective optimization is used to maximize the refinery profit subject to a certain CO_2 reduction target using different mitigating strategies, namely, flow-rate balancing, fuel switching, and CO_2 capturing. The refinery-planning model includes a CDU, different hydrotreaters, a reformer, FCC and HC. However, the CO_2 emissions model was based only on the fuel-firing emissions and did not account for process related emissions.

On the technical side, Greek [8] studied the importance of gasification and pre-combustion processes to reduce refinery CO_2 emissions, and found that capturing processes are more expensive than other carbon management strategies such as improving energy efficiency and shifting to less carbon-intensive fuels to reduce refinery CO_2 emissions. Different strategies for CO_2 emissions reduction in the refinery were evaluated by Moore [9] including online optimization of fuel gas, hydrogen and utility systems. Ritter *et al.* [10] developed a systematic technique for estimating and reporting GHG emissions, especially CO_2, in the oil and gas industry. Metrins *et al.* [11] illustrated an approach for predicting CO_2 emissions. They concluded that rigorous modeling of refinery processes, especially the fractionation columns, conversion reactors and heaters, and including direct and indirect emissions, are required for accurate assessment of CO_2 emissions. Spoor [12] discussed the major contributors to the refinery CO_2 emissions and potential options for emissions reductions. The results of studies conducted at a European refinery are reviewed by Bruna *et al.* [13]. The results showed that significant reductions in CO_2 emissions can be achieved using an optimization approach based on operational improvements and a systematic total site technique. Holmgren and Sternhufvud [14] evaluated different options for CO_2 emissions reduction and the associated costs at petroleum refineries. They concluded that the cost of emissions reduction is strongly dependent on fuel prices and efficiencies of emissions reduction strategies such as carbon capture and storage. Stockle *et al.* [15] used an LP model to identify the best combination of CO_2 emissions reduction schemes to achieve a given reduction in CO_2 emissions including the CO_2 trading price as an operating cost. The emissions reduction schemes considered are efficiency improvement, fuel shifting, carbon capture and sequestration, crude substitution, and hydrogen production. Three emissions sources were included in the LP model, namely; fuel for heat, steam and power provision, hydrogen production, and FCC coke combustion. Ratan and Uffelen [16] claimed that 45% reduction in refinery CO_2 emissions can be achieved by implementing appropriate improvements in the hydrogen plant. Different strategies for refinery emissions reduction were also discussed by Mertens and Skelland [17] including utility optimization and cogeneration. Carter [18] emphasized the importance of energy management in improving refinery margins and reducing CO_2 emissions.

Despite the contributions of these academic and technical studies to the optimization of CO_2 emissions in the petroleum refinery, the tradeoff between CO_2 emissions and operating and economic objectives was not properly addressed in these studies due to the use of single-objective optimization. Furthermore, simple LP was often used to simulate the refinery processes, which may omit important process features and may not adequately reflect the full picture of the refinery. More work, therefore, needs to be done on targeting CO_2 emissions in the refinery using rigorous and comprehensive optimization approaches.

The majority of CO_2 emissions from refineries come from just a few main units such as crude distillation, catalytic cracking and hydrotreating [12]. These units are also the

major energy consumers due to the considerable amount of energy used including fuel, electric power and steam. Significant energy savings in such energy-intensive units can be obtained via improvements in waste heat recovery to minimize total energy consumption [17]. Energy integration technology has been proven to be successful in minimizing total energy requirement and reducing consequential emissions.

In particular, pinch analysis has been proven to be an efficient tool in developing an inherently energy-efficient design of integrated processes for both new plants and retrofits [19–25]. However, the degree of heat integration is often limited by many practical and operational constraints. Furthermore, different levels of energy integration might lead to very different economic and environmental effects. Therefore, the optimum level of energy integration can only be determined by simultaneously considering different impacts on the process. For such problems, multi-objective optimization (MOO) needs to be used, where a set of equally good solutions is produced. These solutions, referred to in the MOO community as the Pareto-optimal front, provide greater insight and enhance the decision-making process.

A new MOO framework to target CO_2 emissions is presented in this chapter. Direct and indirect sources of CO_2 emissions, including emissions from fuel consumption and the provision of heating and cooling utilities, are considered. Unlike some of the previous studies, the two refinery units considered in this study, namely, the crude distillation unit (CDU) and the fluidized-bed catalytic cracker (FCC), are modeled rigorously. Different objectives are simultaneously optimized in two bi-objective problems to investigate the best trade-off targets. The two refining units are presented in the next section, and this is followed by a brief overview of pinch analysis and MOO. Next, the MOO framework is presented and then applied to two different case studies. More modeling details of the two processes are provided in Appendix 11.A1.

11.1.1 Overview of the CDU

The CDU is the first major unit to process petroleum in any refinery. Its objective is to separate crude oil into appropriate fractions, such as naphtha, kerosene, diesel, gas oil, and atmospheric residue, according to their boiling points, to be further treated in downstream processes. Figure 11.1 shows the process flow-diagram of a CDU. Firstly, the crude oil from storage tanks is preheated by a series of heat exchangers. A Desalter is installed in the heat-exchanger train to reduce the salt content of the crude by an electric desalting process. Then, the desalted crude is further heated and sent to a preflash tower where vapors are separated from the liquid feedstock to reduce the vapor pressure of the crude and decrease the vapor load on the atmospheric column. A fired heater is used for further heating the preheated crude before entering the atmospheric column where the fractionation occurs.

Naphtha is produced as a vapor and condensed by the overhead condenser. Kerosene, diesel, and atmospheric gas oil (AGO) are withdrawn as side streams and further refined using side columns, which are either reboiled or use stripping steam, to reduce the content of the lighter components in each product. These products are sent for processing in other downstream units to increase the value of the final products whilst the atmospheric residue is further distilled under vacuum conditions to achieve the required separation between the heavy components at lower temperatures. A stripping steam is injected at the bottom of the vacuum tower to lower the bottom temperature and avoid degradation. The main products

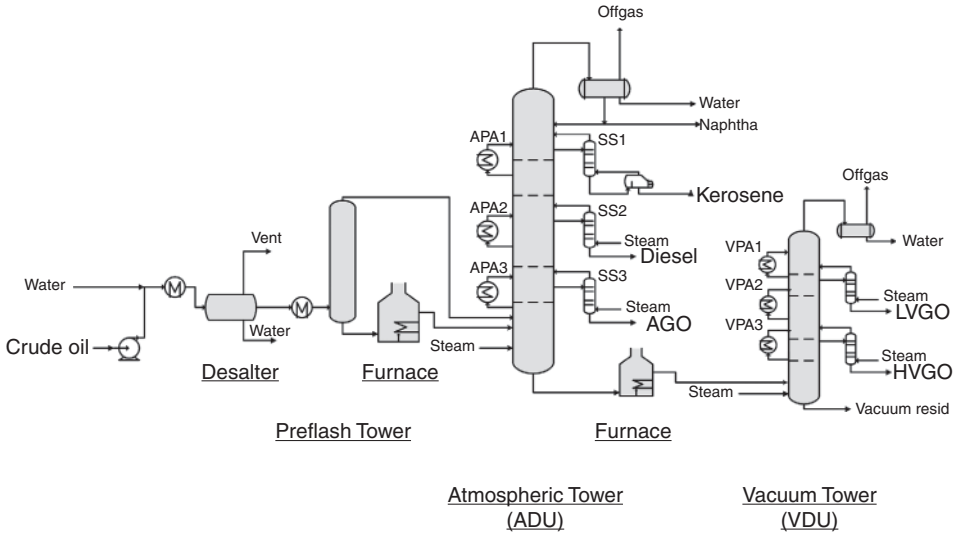

Figure 11.1 *Process flow-diagram of the crude distillation system.*

from vacuum distillation are: overhead gases, light vacuum gas oil (LVGO), heavy vacuum gas oil (HVGO) and vacuum residue. Similar to the atmospheric column, pump around circuits are used to minimize the internal vapor-liquid traffic variations throughout the column and to recover heat at a higher temperature than the condenser [26]. Furthermore, waste heat is recovered from the products before sending them to downstream processes. LVGO and HVGO are sent to the catalytic cracking unit to produce more gasoline and diesel cuts.

As mentioned earlier in this chapter, the CDU is one of the largest energy consumers in the refinery and hence a significant contributor to CO_2 emissions in the refinery [12]. However, potential reduction in CO_2 emissions and energy efficiency opportunities can be brought by maximizing waste heat recovery and heat integration [23, 25, 27, 28]. The latter can be further enhanced by the integration of the CDU and other units of the refinery such as the FCC [29].

11.1.2 Overview of the FCC

The objective of the FCC is to convert heavy petroleum cuts such as AGO, vacuum gas oil and residue into more valuable, lower molecular-weight products such as gasoline, diesel and light products. Due to its significant effects on refinery profitability, the FCC has become the heart of the modern refinery, and profit optimization of FCC units has become a major concern for many petroleum refineries.

Figure 11.2 shows a simplified process flow-diagram of a typical FCC unit. After being heated by a preheat train and a fired heater, the FCC feedstock is injected into the bottom of the riser. Once it contacts the hot reactivated catalyst flowing from the regenerator, the liquid feed is vaporized and then cracked inside the vertical riser pipe to produce lighter products. The reaction products and the catalyst leave the riser to the disengager vessel

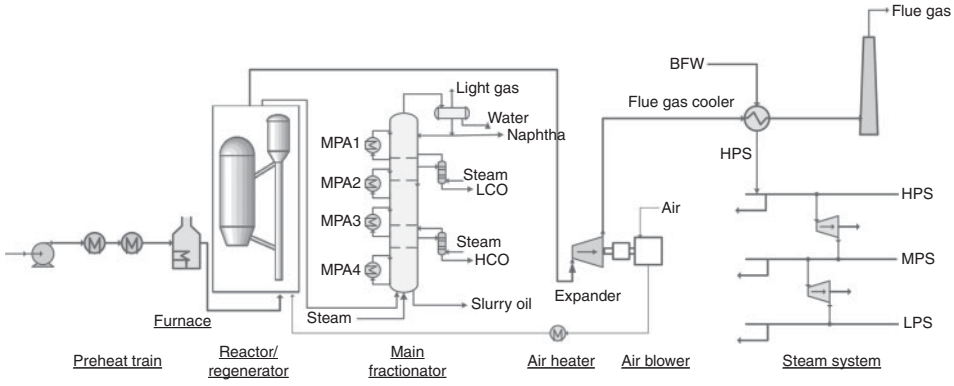

Figure 11.2 *Process flow diagram of the FCC.*

where they are separated. The products are sent to the main fractionator for separation while the spent catalyst is returned to the regenerator for restoring its catalytic activity.

In the regenerator, hot air from a main blower is mixed with the spent catalyst to burn off the coke from the catalyst. As a result of the combustion process, pressurized hot flue gas consists mainly of CO_2, CO and water vapor. An expansion turbine is used to reduce the high pressure of the flue gas and to generate electric power to run the main air blower, while a waste heat boiler is used to generate high-pressure steam from the hot, depressurized flue gas.

In the main fractionator, the reaction products from the reactor are separated into various products, namely, light gases, naphtha, light cycle oil (LCO), heavy cycle oil (HCO), and slurry oil. The fractionator is equipped with pump arounds, side strippers for LCO and HCO products, and the overhead reflux system.

The FCC is one of the major sources of greenhouse gas emissions in the refinery, especially CO_2. The majority of CO_2 emissions comes from the catalyst regenerator where coke on the spent catalyst is burnt off to restore the catalyst activity and provide the heat required for reactor/riser reactions. However, only quarter of the heat available from coke combustion is used for the endothermic reactions, whilst a significant amount of heat is lost to the atmosphere mainly via flue gas [17]. Further, the FCC indirectly contributes to the global CO_2 emissions due to utilities consumptions such as steam and electric power. Different areas for potential reduction in CO_2 emissions associated with the FCC have been investigated in recent studies [17, 19, 30]. According to these studies, a significant reduction in CO_2 emissions from the FCC can be achieved by increasing heat integration and power recovery [29]. This can be achieved using different improvements such as installing a power recovery turbine and increasing or changing the number of pump around circuits.

11.1.3 Pinch Analysis

Pinch analysis is a method for analyzing and enhancing energy efficiency within process design and operation. The technique was first introduced in 1979 by Linhoff and co-workers

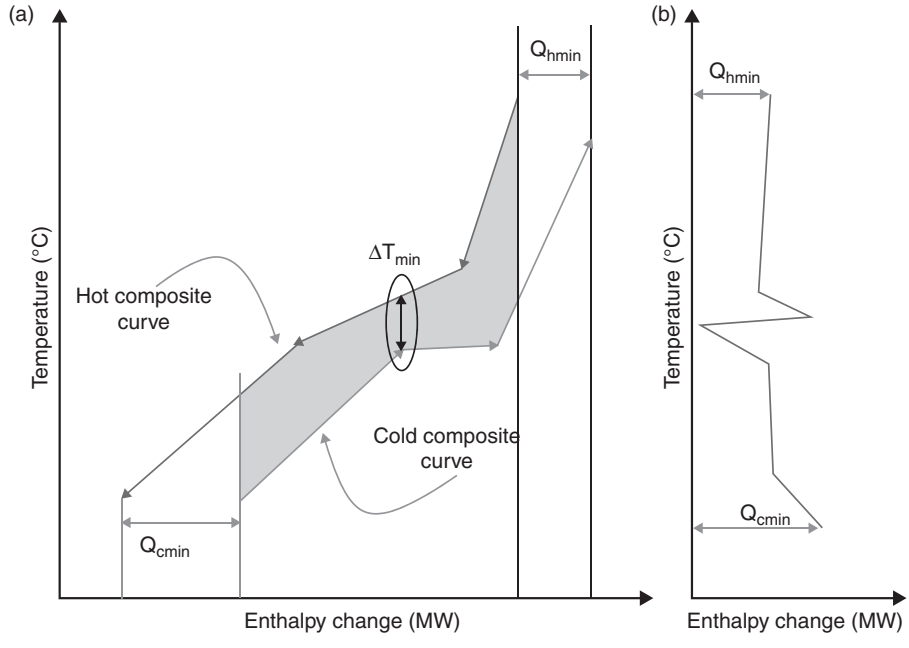

Figure 11.3 *Composite and grand composite curves.*

to analyze energy flows in process heat-exchanger networks. It is based on the second law of thermodynamics, which states that heat can only flow from higher temperatures (sources) to lower temperatures (sinks) [31]. A set of simple graphical tools is used to demonstrate the thermodynamic limits to heat integration, which can be achieved by maximizing process-to-process heat recovery and minimizing external energy consumption. Many improvements and additions have been introduced to pinch analysis leading to better utilities placement in processes where co-generation must be taken into account [32]. Pinch analysis can be applied to individual processes to set a target for internal energy consumption, or to a total site to optimize site-wide energy consumption [21]. Some concepts and tools of pinch analysis that are employed in this chapter are briefly described below. A pinch analysis example is illustrated in Appendix 11.A3, and complete details on pinch analysis can be found in Smith [32] and Kemp [33].

11.1.3.1 Composite and Grand Composite Curves

The target for minimum energy consumption is obtained by using a graphical tool of pinch analysis, known as the composite curve (CC) (Figure 11.3a). In this diagram, all the hot streams are lumped together in terms of heat load and temperature level, into one hot CC (heat source), and cold streams are similarly lumped into one cold CC (heat sink). When the heat source and sink curves are plotted on a temperature–enthalpy graph, targets for the heat deficit (Q_{hmin}) and surplus (Q_{cmin}) can be determined as shown in Figure 11.3a. The

CC also shows the heat recovered within the process as the overlapping portion of the two curves. The minimum temperature approach between the two CCs must be greater than or equal to a specified temperature approach (ΔT_{min}), see Figure 11.3a. As the ΔT_{min} is increased (the cold curve is moved to the right), the heat recovery region reduces and the utility requirements increase. ΔT_{min} is usually set by the economics of a given process and should be reviewed, when economic conditions change. The shaded area in Figure 11.3a between the hot and cold CCs can be used to calculate the minimum heat transfer area required for maximum heat recovery.

The grand composite curve (GCC) is another graphical pinch analysis tool and is constructed from enthalpy differences between the composite curves after vertically shifting the hot CC by ($-\frac{1}{2}\ \Delta T_{min}$) and the cold CC by ($+\frac{1}{2}\ \Delta T_{min}$). A typical GCC is shown in Figure 11.3b. Enthalpy in the x-axis of GCC refers to the enthalpy difference between CCs after shifting. The horizontal arrows in Figure 11.3b show the minimum heating, Q_{hmin} and cooling, Q_{cmin} duty required.

Often, several utilities are available at different temperature levels to fulfill the external heating and cooling requirements of the system. The most appropriate set of utilities required can be best judged using GCC (Figure 11.3b) by matching available utilities against the process profile to meet the net heat requirements and minimize the consequential operating cost. This is achieved by minimizing relatively expensive utilities such as high-pressure steam and refrigeration, while maximizing the use of cheaper utilities such as low-pressure steam and cooling water. Similarly, utilities consumption can be optimized using the GCC to target consequential CO_2 emissions.

The first step in matching utilities is to set ΔT_{min} for the process-utility heat exchangers. For a heating application, this parameter represents the minimum allowance between the hot utility and the cold process stream in the heater. Different values of ΔT_{min} can be used for different utilities, and typically a higher value of ΔT_{min} is used when heating with flue gas than with steam, due to flue gas being a low-pressure gas stream with poor heat transfer characteristics. Similarly, in a cooling application, ΔT_{min} is the minimum allowance between the cold utility and the hot process stream, and again typically a higher value of ΔT_{min} is used when cooling with re-circulated cooling water than with refrigeration, but this time the reason is the high operating and capital costs of refrigeration.

The available utility levels are then matched against the GCC in order to meet the total energy requirements. The targeting process for multi-level utilities starts by maximizing the use of the cheapest utility first (providing that it is available) then moving to the next cheapest level and so on until the net energy demands are satisfied [33]. Figure 11.4 shows a typical GCC after multi-level utilities have been matched. Furnace flue gas or a hot oil circuit is normally used for high-temperature heating duties. Lower temperature heating can be provided by a saturated steam at different temperature levels such as low-pressure steam (LPS), medium-pressure steam (MPS) and high-pressure steam (HPS). Based on the range of temperature of the GCC section below the pinch point, different cooling utilities might be used such as cooling water (CW), air cooling, boiler feed water (BFW) and refrigeration. Similarly, with cold utilities, the cheapest utility would be consumed first (air or water cooling), before chilled water or refrigeration. Utilities with only sensible heat such as flue gas and cooling water are represented by sloping lines whereas horizontal

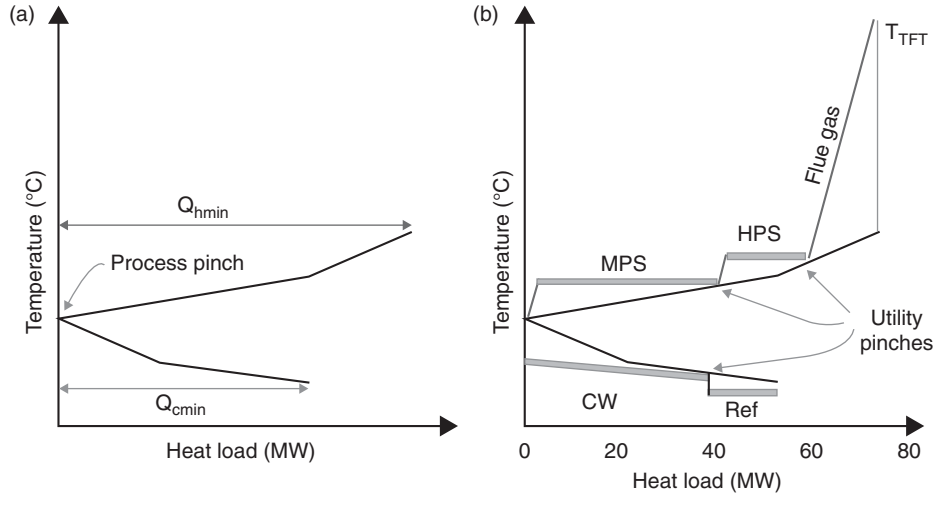

Figure 11.4 *GCC with utility distribution: (a) before and (b) after matching multi-level utilities.*

lines are used to represent single-component utilities that absorb or liberate their latent heat during condensation or boiling such as saturated steam and pure refrigerants. The utility pinch points, as shown in Figure 11.4, occur when the maximum heat duty is used at each utility level. Once the different utilities have been matched against the GCC and the load of each utility has been determined, details of different utilities, including their marginal costs and consequential emissions, are used to estimate the operating cost and total emissions of the utility system.

11.1.3.2 Total Site Pinch Analysis

There are two modes of heat integration for a site with multiple processing units. First, there is direct integration where all hot and cold streams from different processes are assumed to be available. In this case, the minimum heating and cooling demands and the best application for utilities can be determined using CC and GCC of the integrated processes, identical to a single processing unit. However, direct integration assumes that different processes will never be operated independently of each other so that heat is always available to be transferred. Often this is not the case and the utility system is required to compensate. Therefore, a more practical approach is indirect integration, or so-called total site heat recovery [34], where pinch analysis is applied to individual processes in order to maximize heat recovery and these processes are then linked to the same utility system. Figure 11.5 shows a schematic of a multi-process site involving three different processes. Both consumption and generation of utilities such as steam and cooling water from processes are linked through a central utility system. A main steam boiler is used to supply the steam at different mains and co-generate power via expansion turbines. The power is imported or

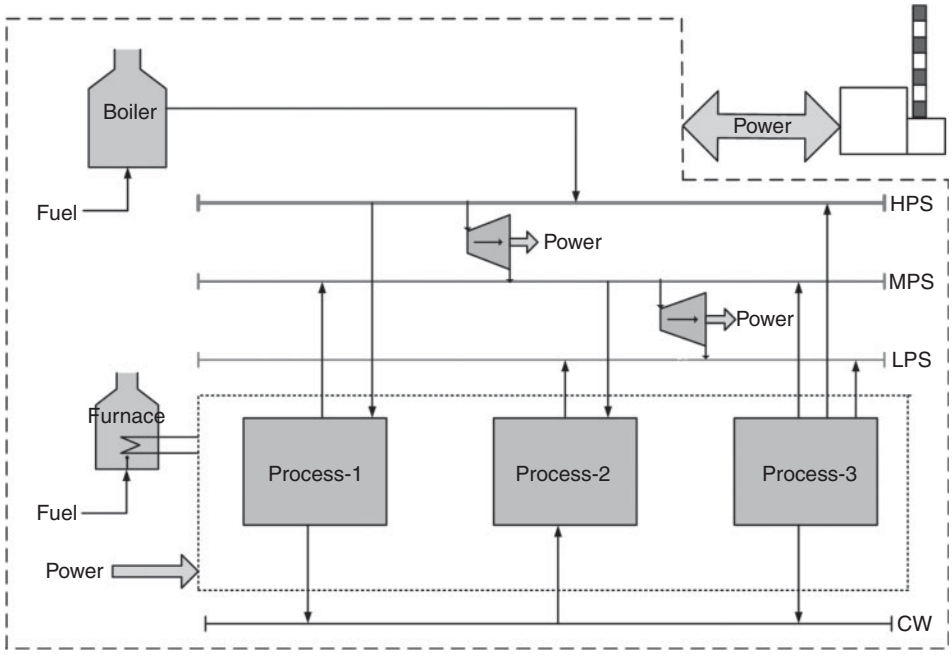

Figure 11.5 *Schematic of a utility system in total site mode.*

exported by the site to balance the on-site power-generation/consumption. Process furnaces are used whenever direct heating is required within the processes.

The total site heat recovery is performed by identifying the net heat sources and sinks from the GCC of each individual process (Figure 11.6). The net heat sources and sinks for each process are the remaining parts of the GCC after excluding the process-to-process heat-recovery pockets from each individual GCC [20]. Figure 11.6 demonstrates the construction of total site profiles from individual GCCs of three different processes. The net heat sources from individual GCCs are combined into the total site heat source profile whereas the total site heat sink profile is constructed by combining net heat sinks from individual GCCs as shown in Figure 11.6. Then, the resulting profiles of the total site heat sources and sinks are vertically shifted by $-\frac{1}{2}\ \Delta T_{min}$ and $+\frac{1}{2}\ \Delta T_{min}$, respectively, in order to shift the temperature to provide the additional driving force required when using a heat transfer medium to transfer the heat from a process source to a process sink. The total site composite curves represented by the total site heat source and sink profiles show opportunities for heat recovery using steam mains.

11.1.4 Multi–Objective Optimization (MOO)

The subject of this book, MOO is used in the simultaneous optimization of several objectives. Often, these objectives are noncommensurable and come into conflict with one

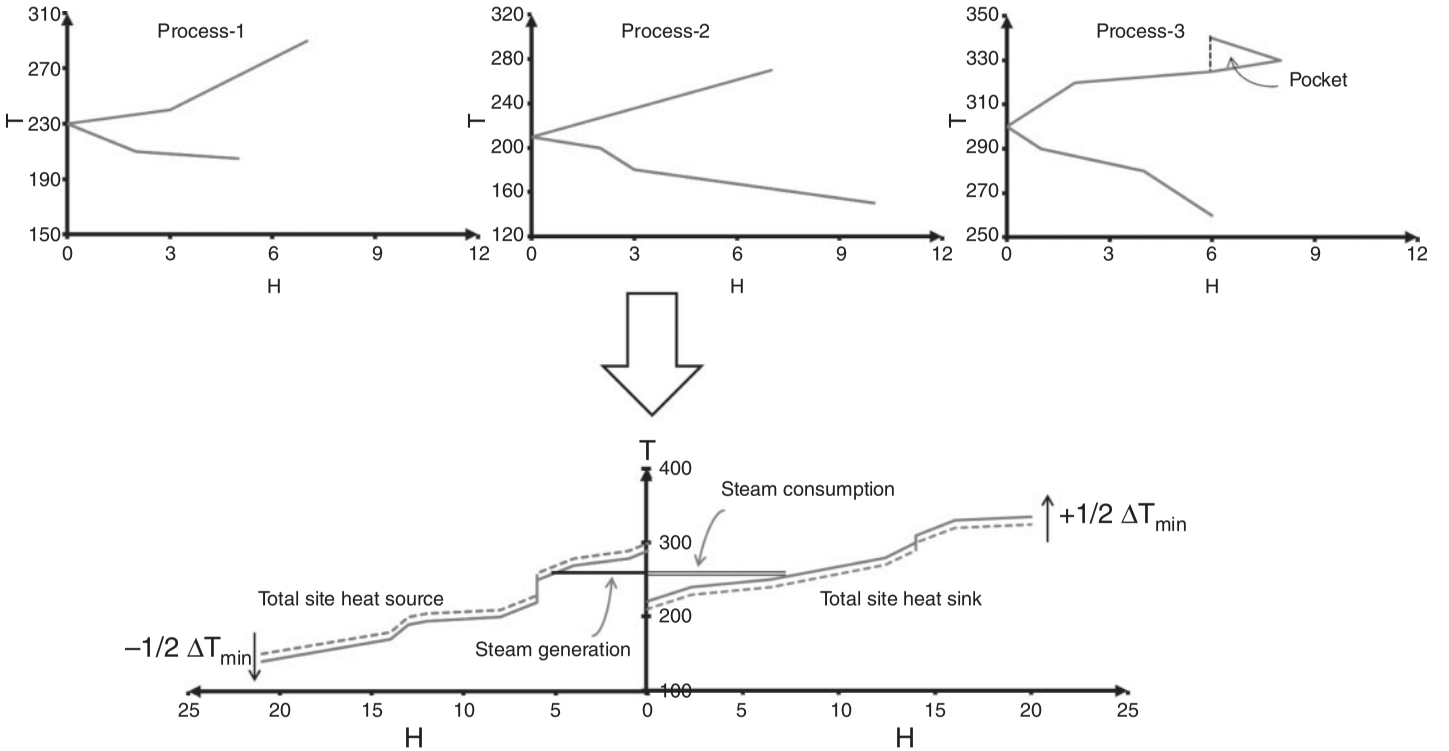

Figure 11.6 *Construction of the total site profiles.*

another, and so there is no single optimum. Minimizing CO_2 emissions, for example, may affect other objectives like profit and product yield, and so compromises must be made. Optimal solutions of MOO are a set of non-dominated solutions called Pareto-optimal solutions. The non-dominated solutions mean that every solution is better than others in at least one objective and worse than others in at least one other objective.

Numerous studies have been reported in the MOO area since the early 1990s. These include many different chemical engineering applications [35]. Multi-objective optimization has been applied successfully to a number of petroleum-refining operations. Different objectives have been optimized, such as product yields, capital cost and profit. Despite recent studies, which applied MOO to different refinery processes [27, 30], heat integration of multiple processes on a site and the resulting impacts on environmental targets are still to be investigated. In this chapter, MOO is used in conjunction with both steady-state process simulation and pinch analysis to investigate the tradeoffs associated with different levels of CO_2 emissions.

11.2 MOO-Pinch Analysis Framework to Target CO_2 Emissions

The framework for CO_2 targeting using pinch analysis and MOO is shown in Figure 11.7. The first step starts with simulating the process using a simulator such as Aspen HYSYS®, for the given values of decision variables. Then, objectives, decision variables, constraints and stream data are transferred to the spreadsheet within Hysys, which is used as an interface between the process simulator and the Excel-based optimization algorithm, which is a binary coded elitist Non-dominated Sorting Genetic Algorithm (NSGA-II) [36]. Once the process simulation is converged, temperature-enthalpy data of all streams are transferred from the Hysys spreadsheet to the VBA-based program for pinch analysis. The CC and GCC are constructed using this VBA program to find the heating and cooling demands as well as the target for each utility level. Pinch analysis results are sent back to the Hysys spreadsheet to calculate the objectives. Then, values of objectives and constraints for the given values of

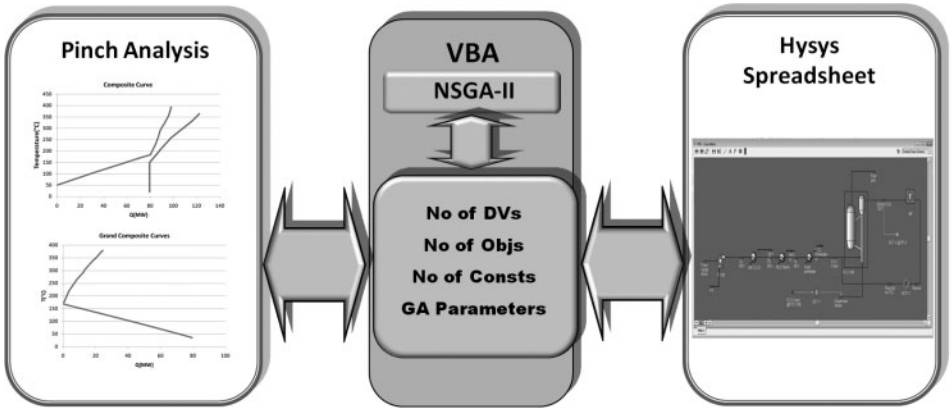

Figure 11.7 *Framework for MOO-pinch analysis and construction of the total site profiles.*

decision variables are exported from Hysys spreadsheet to NSGA-II, to produce the next trial solution (i.e., values of decision variables) by the optimization algorithm. These steps continue until the maximum number of generations (Figure 11.7).

11.3 Case Studies

In this section, MOO-pinch analysis framework is demonstrated using two different case studies of bi-objective optimization. The total yield of naphtha from both the CDU and FCC, Equation (11.1), is used as an economic objective to be maximized while minimizing the total CO_2 emissions (the environmental objective), Equation (11.2). Total CO_2 emissions include emissions from furnaces, boilers, power importation and the FCC regenerator. These emission values are calculated by Equations 11.3 to 11.5. An Australian black coal is assumed to be used in the central power station with an emissions factor of 0.92 tonnes CO_2/MWh [37]. In the first case study, direct heat integration of the CDU and FCC units is permitted, while the second study is on a total site integration, which only allows the exchange of heat between the CDU and FCC unit via the utility system.

$$Naphtha\ yield = (CDU\ Naphtha + FCC\ Naphtha)/Crude\ feed \tag{11.1}$$

$$CO_2 emissions = \left(CO_{2(Furnaces)} + CO_{2(Boilers)} + CO_{2(power)} + CO_{2(FCC)}\right)/Crude\ feed \tag{11.2}$$

$$CO_{2(Furnaces)} \text{ or } CO_{2(Boilers)} = Q_{Fuel} E_{Fact} \tag{11.3}$$

$$E_{Fact} = (RC/NHV)\,(C\%/100) \tag{11.4}$$

$$CO_{2(power)} = [Power\ (MW)]\ [power\ emission\ factor\ (= 0.92)] \tag{11.5}$$

In the above equations, Q_{Fuel} = heat duty supplied by fuel (kJ/h), E_{Fact} = emission factor for a specific fuel (kgCO_2/kJ), RC = molar mass ratio of CO_2 and C (=3.67), NHV = net heating value of the fuel (kJ/kg) and C% = carbon mass percent in fuel.

During the optimization, 16 decision variables are allowed to vary, each within a realistic range, to achieve optimum values for the objectives. These variables have been chosen from operating variables that have direct impact on both objectives. The decision variables and their bounds are listed in Table 11.1. The objective functions are optimized, subject to relevant constraints to be kept within the defined bounds (Table 11.2). In order to maintain specifications of products, the boiling point gaps between different products of the CDU are kept within acceptable ranges given in [38]. The remaining coke on the regenerated catalyst and maximum regeneration temperature must be constrained to maintain activity and avoid the decomposition of catalyst [39]. The concentration of CO in the regenerator flue gas must be as low as possible for full combustion mode regeneration to ensure complete combustion inside the regenerator and minimize pollution [39].

Preliminary numerical experiments in order to select the appropriate NSGA-II parameters are shown in Appendix 11.A2. Values of computational parameters in the NSGA-II algorithm used are: random number seed = 0.857, crossover probability = 0.8, mutation probability = 0.05 and population size = 50. Around 200 generations are required to provide a smooth set of Pareto optimal solutions; see Figures 11.A1 to 11.A4.

Table 11.1 *Decision variables and their bounds.*

Decision variable	Units	Lower bound	Upper bound	Type
ADU feed temperature (AtmT)	°C	350	380	Continuous
Light crude fraction		0.1	0.9	Continuous
Kerosene reboiler duty (KerRQ)	GJ/h	10	100	Continuous
VDU feed temperature (VacT)	°C	360	400	Continuous
FCC feed temperature (FCCT)	°C	380	400	Continuous
Riser temperature	°C	480	520	Continuous
ADU PA3 return temperature (APA3T)	°C	250	300	Continuous
ADU PA3 flow rate (APA3F)	m^3/h	150	300	Continuous
VDU PA3 return temperature (VPA3T)	°C	280	320	Continuous
VDU PA3 flow rate (VPA3F)	m^3/h	100	200	Continuous
Main fractionator PA3 flow rate (MPA3F)	m^3/h	100	400	Continuous
Main fractionator PA3 temperature drop (MPA3DT)	°C	30	100	Continuous
Main fractionator PA3 draw stage (MPA3DS)		7	10	Discrete
Main fractionator PA4 flow rate (MPA4F)	m^3/h	100	500	Continuous
Main fractionator PA4 temperature drop (MPA4DT)	°C	50	130	Continuous
Main fractionator PA4 draw stage (MPA4DS)		11	13	Discrete

11.3.1 Case Study 1: Direct Heat Integration

This case study involves the direct heat integration of all process streams within the CDU and FCC units. The Pareto optimal solutions obtained by simultaneously minimizing CO_2 emissions and maximizing naphtha product from the integrated model of the CDU and

Table 11.2 *Constraints in the MOO problem.*

Constraint	Specification
Kerosene-Naphtha (5–95) Gap	>16.7 °C
Diesel-Kerosene (5–95) Gap	>0 °C
AGO-Diesel (5–95) Gap	>–11 °C
Coke on reg. catalyst	<0.1 wt%
Regeneration temperature	<717 °C
CO in the flue gas	<0.2 wt%

FCC are shown in Figure 11.8a. Values of decision variables corresponding to the Pareto set are shown in Figures 11.8b to 11.8q.

Figure 11.8a shows the contradictory behavior of the two objectives—while maximizing naphtha product, more CO_2 emissions are expected. Results in this figure show that a 24% increase in total naphtha product results in a 39% increase in CO_2 emissions. A vertical

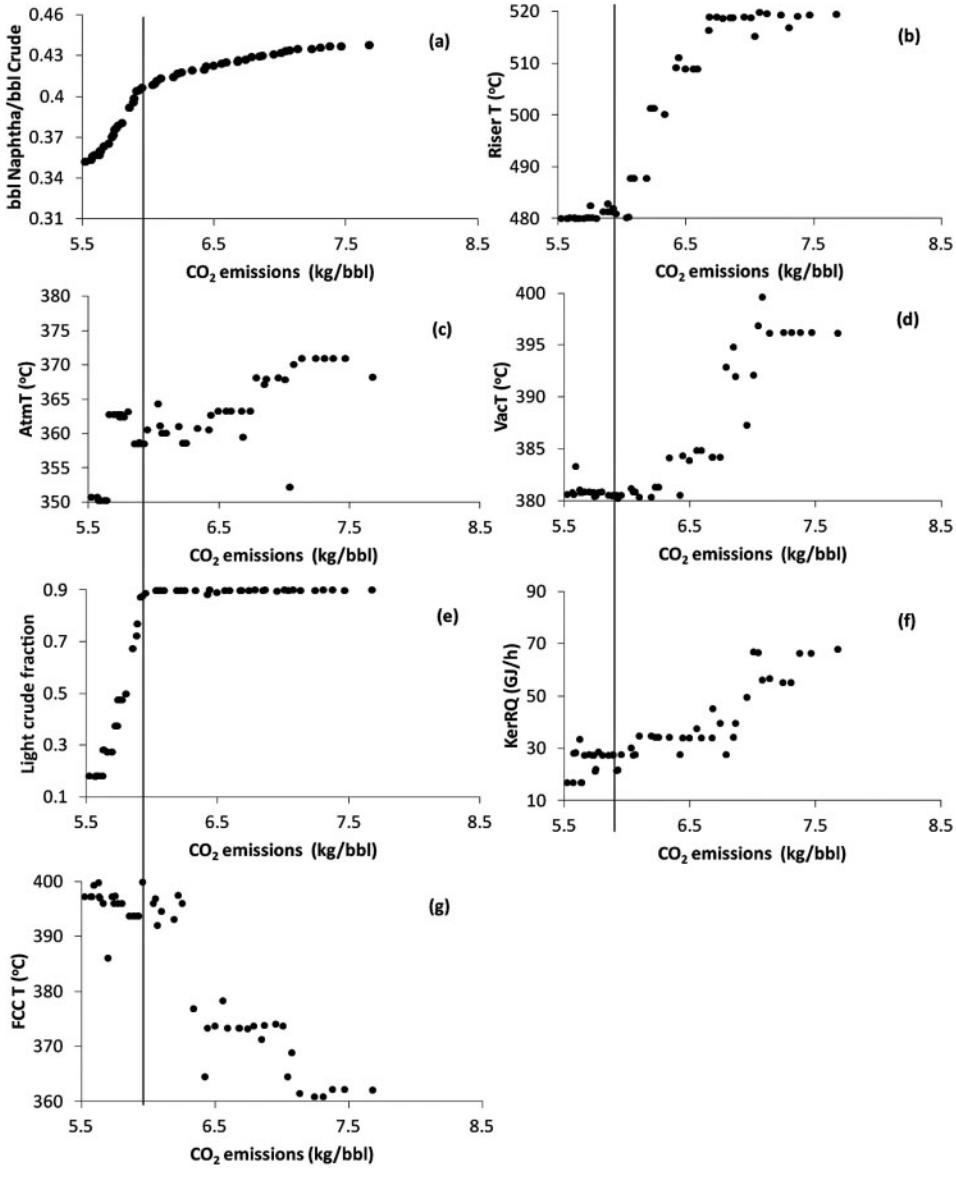

Figure 11.8 *MOO optimization results of direct integration.*

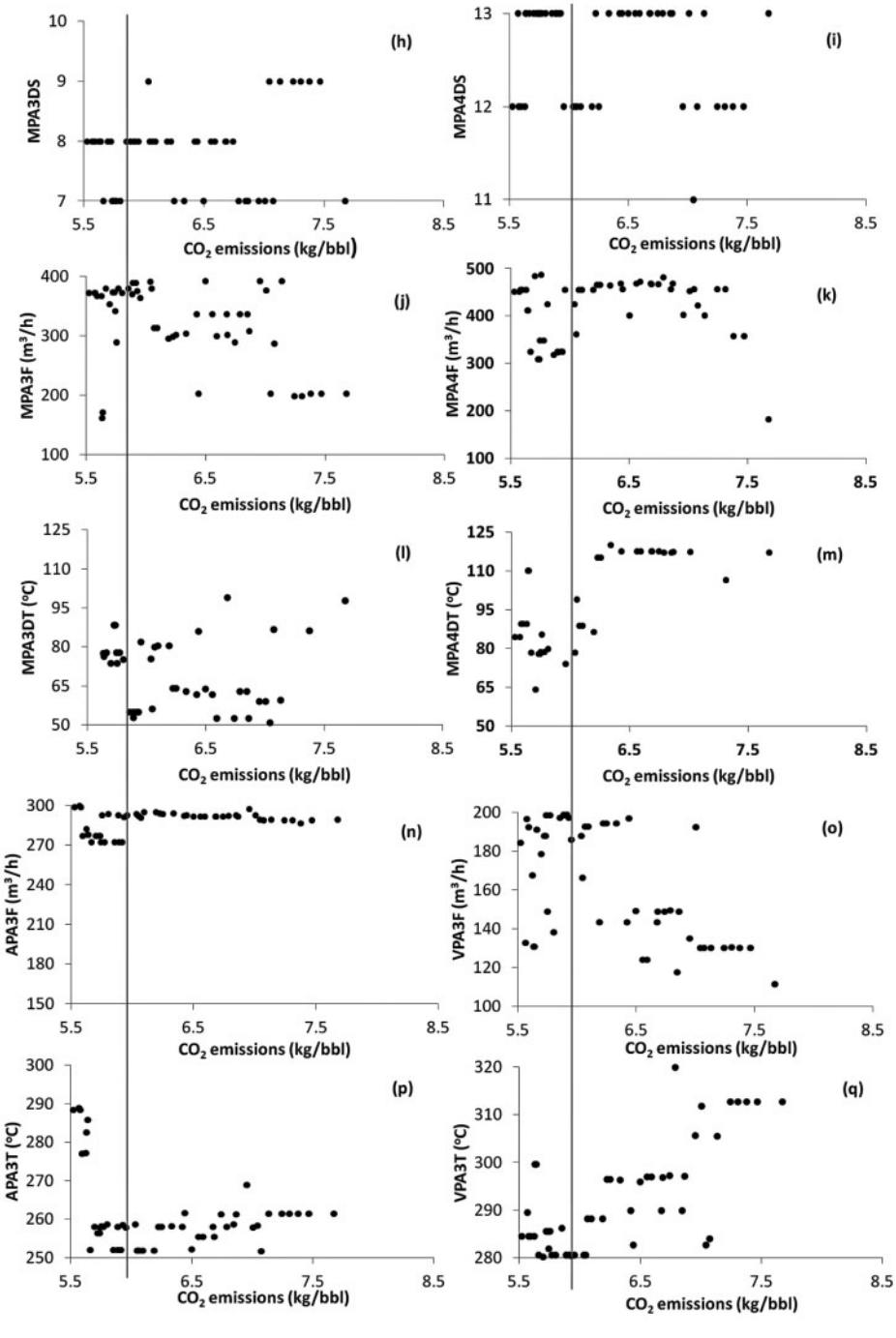

Figure 11.8 *(Continued)*

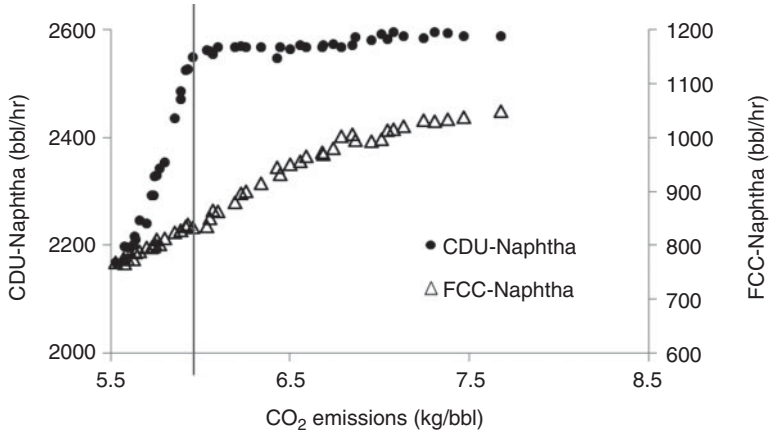

Figure 11.9 *Optimum values of naphtha flow rate from the CDU and FCC.*

line on each plot in Figure 11.8 denotes the boundary between the two main trends in the Pareto-optimal solutions. This boundary is also apparent in the optimal values of decision variables. Figure 11.8e shows the fraction of light crude in the feed to the CDU. Below CO_2 emissions of 6.0 kg/bbl, the fraction of light crude is the major controlling decision variable for the Pareto solutions. It increases from its lower limit of 0.1 to the upper limit of 0.9, and remains at this higher value for the rest of the Pareto range. Below CO_2 emissions of 6.0 kg/bbl, the other decision variables are constant or are scattered without any underlying trend (Figure 11.8). As a result of increasing the light crude fraction, the quantity of naphtha produced from the CDU increases strongly (see Figure 11.9), as would be expected. However, the highest amount of energy is required by the light crude as it contains the greatest amount of distillates, and so Figure 11.10 shows that an increase in CO_2 emissions occurs due to the increase in the furnace duty of the CDU.

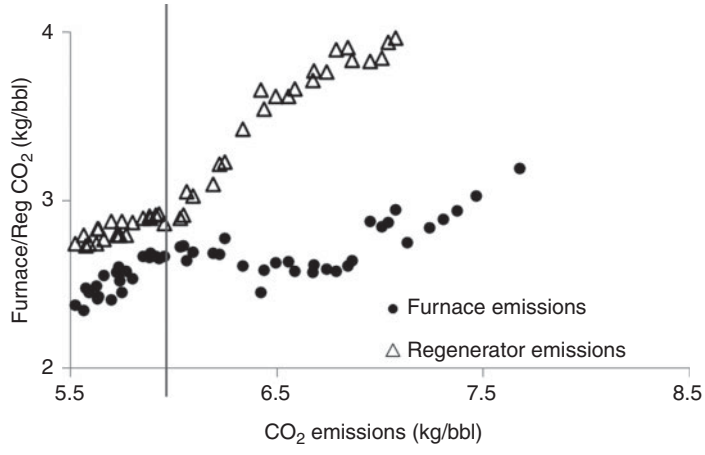

Figure 11.10 *Emissions from the furnace versus emissions from the FCC regenerator.*

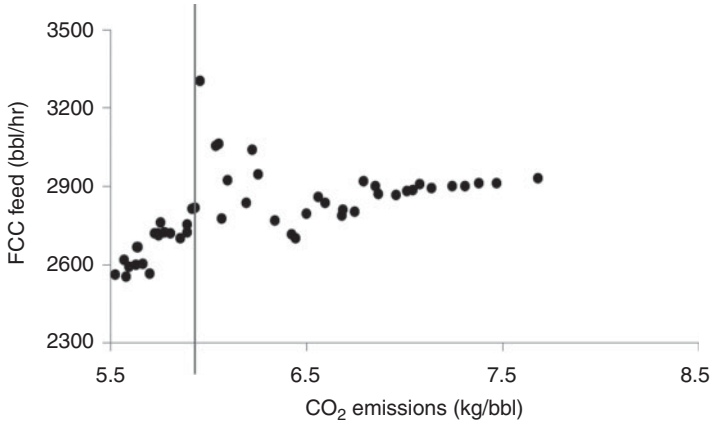

Figure 11.11 *Variation of flow rate of FCC feedstock with CO_2 emissions.*

For optimum solutions with CO_2 emissions more than 6.0 kg/bbl crude, the emissions penalty of increasing naphtha yield increases considerably. Figure 11.9 shows that the increase in naphtha yield in this region of the Pareto-optimal front mainly comes from the FCC unit. Interestingly, most decision variables show significant trends with increasing CO_2 emissions and their optimum values are simultaneously changed throughout this region (Figures 11.8b, d, f and g). Figure 11.8g shows that the FCC feed temperature decreases to its lower limit, while the riser temperature simultaneously increases to its upper limit (Figure 11.8b). This increases the catalyst/oil ratio, which results in higher conversion and consequently higher naphtha yield (Figure 11.9). However, high conversions result in high coke formation, which ultimately increases CO_2 emissions in the flue gas out of the regenerator. Vacuum distillation at a higher temperature increases vacuum gas oil in the FCC feed (Figure 11.11), which also contributes to increasing naphtha yield from the FCC. Furthermore, an increase in the temperature of feed to the atmospheric distillation column and the duty of kerosene reboiler (Figures 11.8c and 11.8f), both result in a slight increase in the yield of naphtha from the CDU (Figure 11.9).

In this case study with direct integration between the CDU and FCC units, the pump-around streams help to preheat the feeds to the CDU and FCC. The decision variables related to pump-around circuits include the draw stage, the flow rate and the change in temperature. In the region above 6.0 kg of CO_2/bbl crude, the pump-around variables show clearer and more dynamic trends (Figures 11.8h to 11.8q). Examining the GCC of the two extreme points on the Pareto-optimal front shows that the return temperature of VPA3 is well above the process pinch point (see Figure 11.12 and Table 11.3). However, the duty of VPA3 decreases along the second part of the Pareto-optimal front (Figures 11.8o and 11.8q). The return stage of VPA3 is located below the draw stage of LVGO and HVGO, which means that decreasing VPA3 duty will increase the yield of LVGO and HVGO products, and consequently the FCC feed flow rate. The results show that optimum withdrawal stages for MPA3 are 7 to 9 whilst stages 12 and 13 are the optimum for MPA4 (Figures 11.8h and 11.8i, respectively).

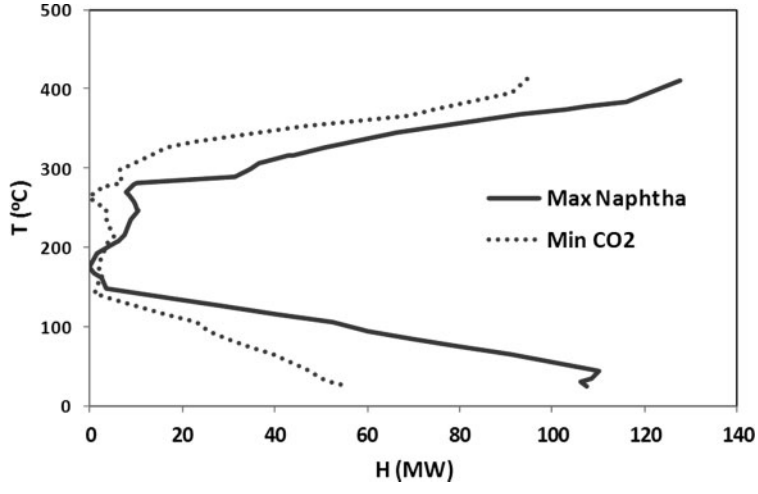

Figure 11.12 *GCC for the extreme solutions of the Pareto-optimal front.*

11.3.2 Case Study 2: Total Site Heat Integration

Figure 11.13 shows the MOO results of the total site integration case, where the integration is limited to the sharing of utilities, particularly, steam. The Pareto-optimal solutions for both cases (direct heat integration and total site integration) are plotted on Figure 11.13a for comparison. Like the direct heat integration case, the Pareto-optimal solutions of the total site show two different trends, for below and above CO_2 emissions of 6.2 kg/bbl crude. The two sets of optimal solutions show that the direct integration has no advantage over the total site case at higher naphtha yield (Figure 11.13a). However, at lower naphtha yield, direct integration results in about 4% lower emission of CO_2 than total site integration, for the same naphtha yield. Most decision variables show similar behavior as in the direct integration case; light crude is the main controller for the first segment of the Pareto-optimal front, whilst the optimum values of the remaining decision variables show trends in the second region of the Pareto-optimal front. The optimum values of all decision variables (Figures 11.13b to 11.13q) have the same trends as in the direct integration case.

In the total site integration case, steam consumption and generation from both the CDU and FCC units are linked to a central utility system. Fired heaters are used for both units wherever high-temperature heating is required, which cannot be supplied by

Table 11.3 *Pump-around return temperatures.*

Specification	For min. CO_2	For max. naphtha
T_{pinch} (°C)	263	175
APA3T (°C)	288	261
VPA3T (°C)	284	312
MPA3T (°C)	229	223
MPA4T (°C)	264	272

steam. As explained earlier in this chapter, the total site profiles are constructed using the individual GCCs of the CDU and FCC units. Any potential generation of high- and medium-pressure steam from the site source profile, if it occurs, is used to fulfill the heating requirements on the site sink profile and the requirements for stripping steam in the CDU and FCC units.

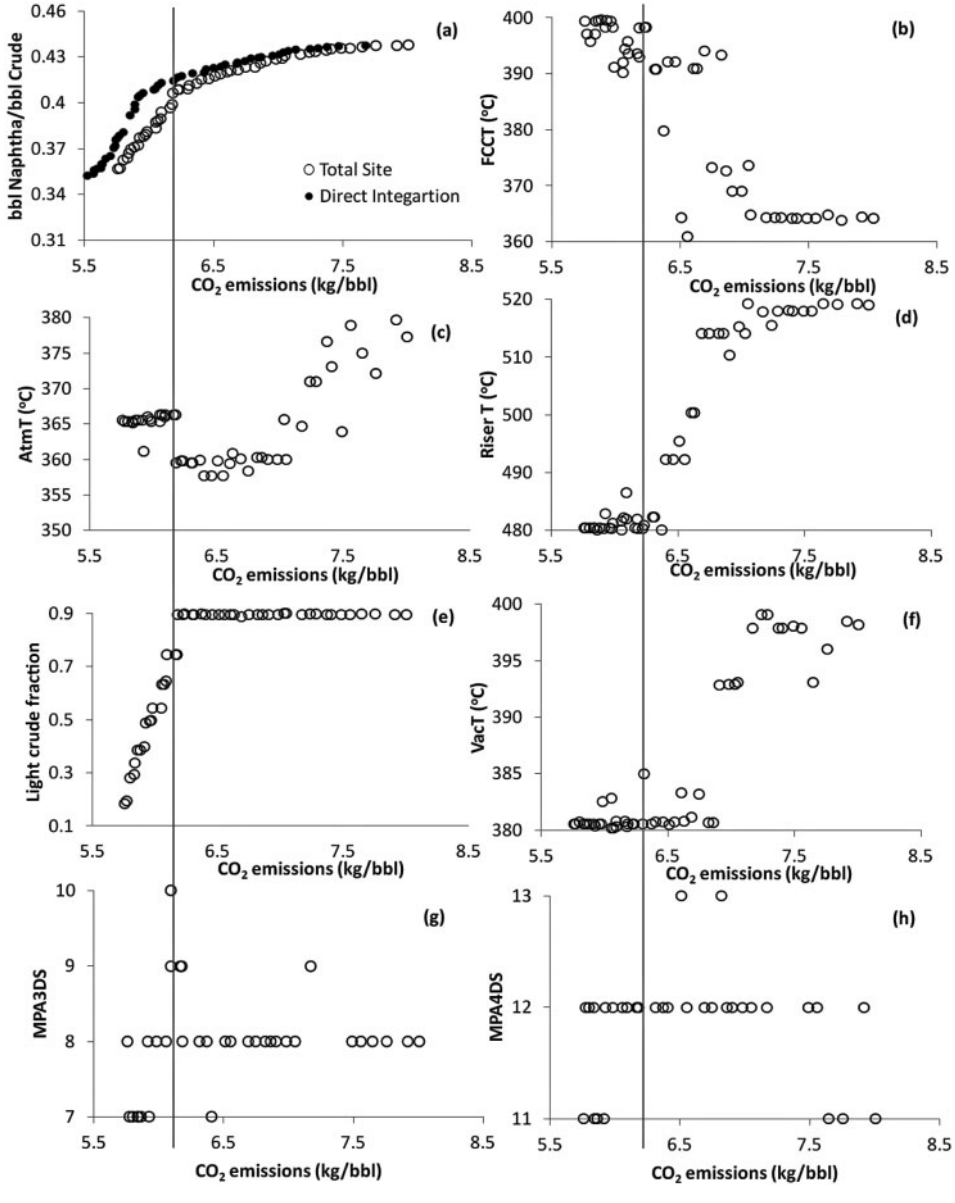

Figure 11.13 *MOO results for total site (indirect) integration. (Continued)*

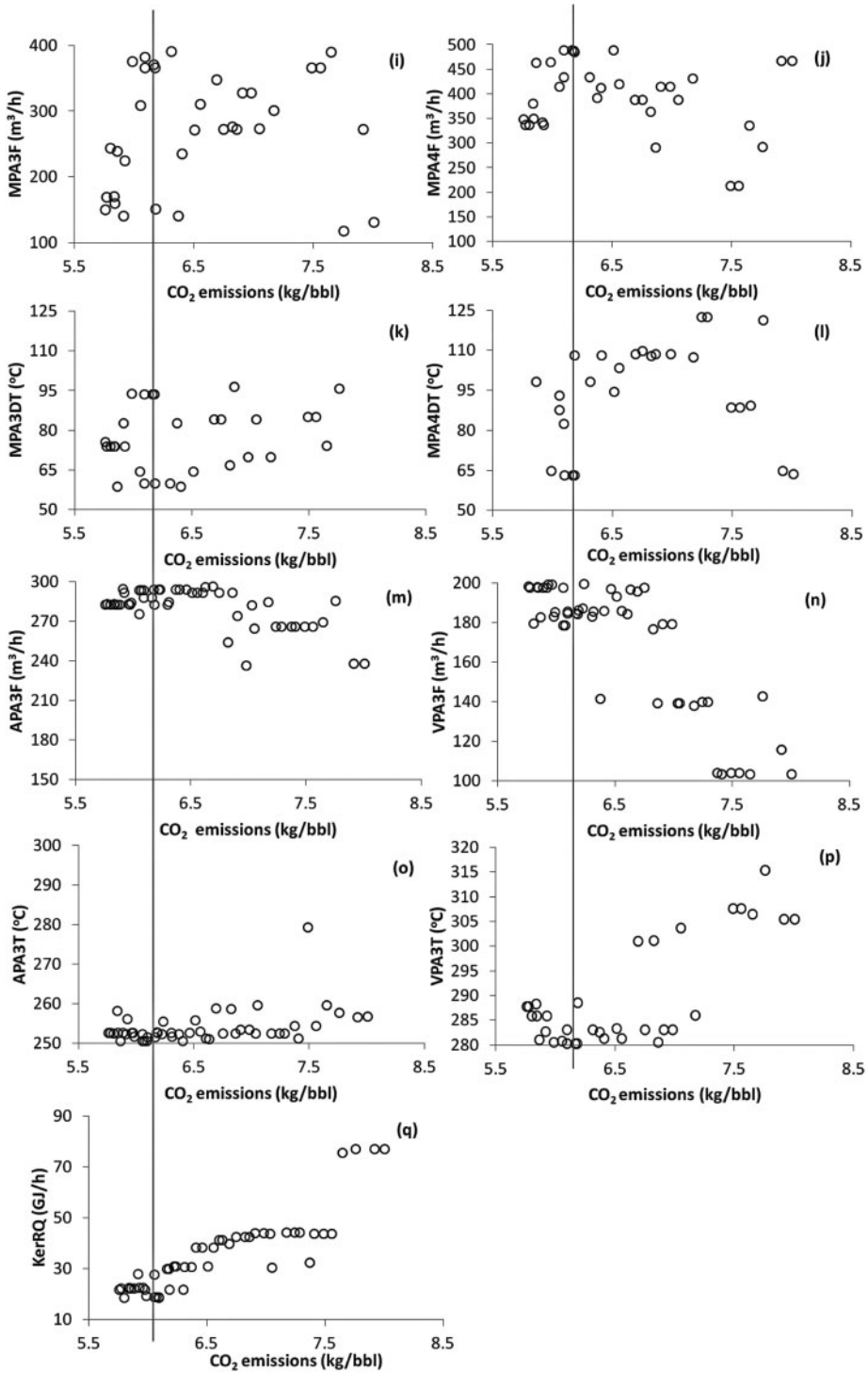

Figure 11.13 *(Continued)*

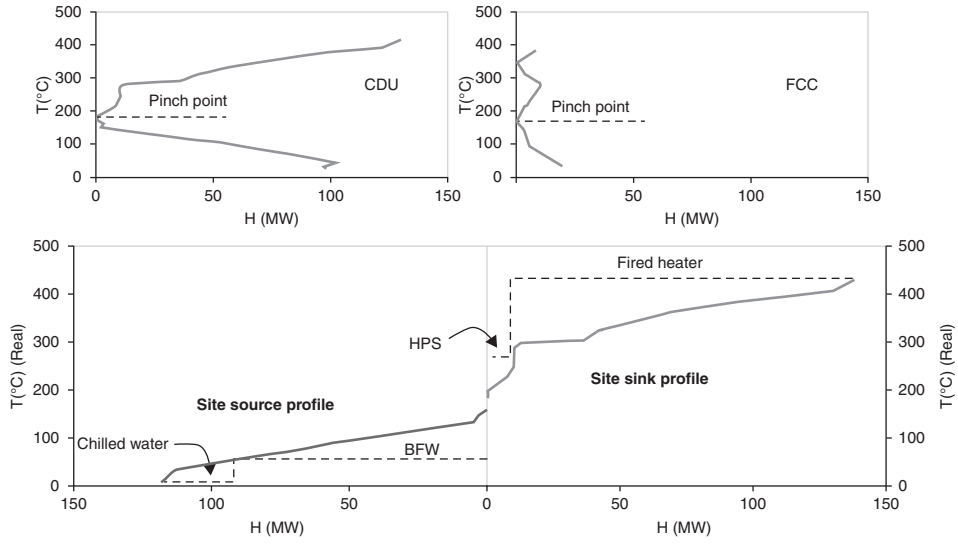

Figure 11.14 *Total site profiles for the maximum naphtha solution.*

For illustration, the total site profiles have been constructed for the two extreme solutions of the Pareto-optimal front: maximum naphtha and minimum CO_2 emissions, and are shown in Figures 11.14 and 11.15, respectively. The GCCs of the CDU and FCC at maximum naphtha show that they both have relatively low process pinch points, 176 °C and 168 °C, respectively. Moreover, it can be seen that the temperature difference between

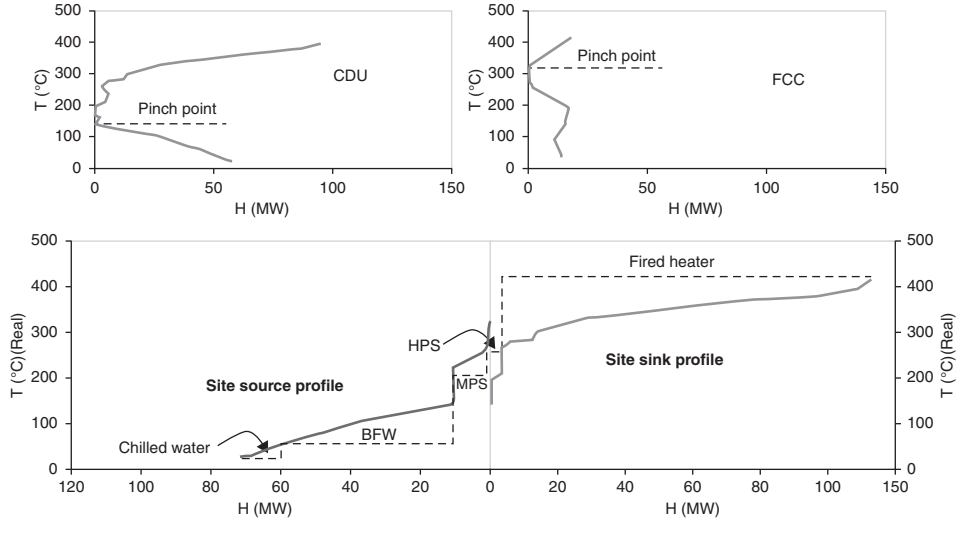

Figure 11.15 *Total site profiles for the minimum CO_2 emissions solution.*

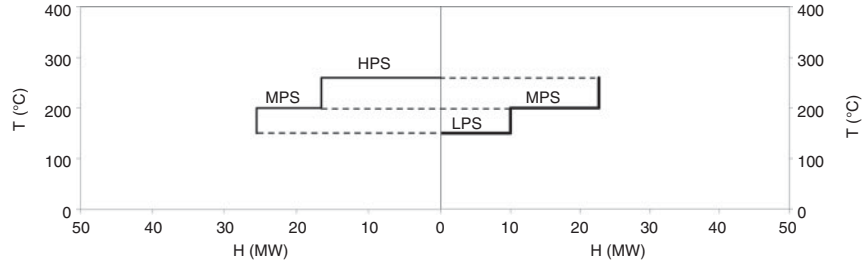

Figure 11.16 *Steam system profile at the minimum CO_2 emissions solution.*

the two pinch points is only 10 °C. This eliminates any opportunity for heat recovery using steam generation (Figure 11.14). In contrast, Figure 11.15 for minimum CO_2 emissions shows that pinch point of the FCC is much higher than that of the CDU which increases the opportunities of heat recovery using HPS and MPS. However, less HPS can be used for heating requirements compared to the maximum naphtha yield (Figure 11.15). Optimizing heating utilities, namely, flue gas eliminates the use of HPS as the heating utility. Figure 11.16 shows the steam system profile at the minimum CO_2 emissions after including steam consumption/generation from Figure 11.15 and stripping steam required.

Table 11.4 compares targets of heat recovery using steam between direct integration and the total site case. Values of total steam consumption shown in this table include stripping LPS and MPS required by the CDU and FCC, and values of HPS generation include steam generation by waste-heat recovery from the regenerator flue gas. For the maximum naphtha solution, there are no significant changes in steam generation, and the consumption between the two cases differs only in that there is a slight increase in HPS and MPS consumption in the total site mode. However, a significant increase in MPS generation can be observed in the total site mode at the minimum CO_2 emissions solution, which partially offsets the requirements for MPS for stripping in the CDU and FCC. Compared to the direct integration case, Table 11.4 shows that the fired heater duty increases by 6% in the total site case at maximum naphtha while this increase escalates to 19% at minimum CO_2 emissions. This shows the effects of the direct integration of process streams on the heat recovery within the CDU and FCC units. However, the increase in the fired heater duty is offset by the larger opportunities for steam generation/consumption in total site case.

Table 11.4 *Targets of steam consumption and generation (in MW).*

	Maximum naphtha		Minimum CO_2 emissions	
Quantity	Direct integration	Total site	Direct integration	Total site
Fired heater duty	127	135	94.6	113
HPS generation	17.2	17.2	15.6	16.6
HPS consumption	0.4	2	0	0
MPS generation	0	0	0.8	9
MPS consumption	15.3	17.1	12.6	12.7
LPS consumption	9.1	9.1	10	10

11.4 Conclusions

In this chapter, a comprehensive MOO framework is introduced to find the Pareto-optimal solutions that describe the tradeoff between economic objective(s) and CO_2 emissions associated with energy use in chemical processes. The optimization framework enables better targeting of CO_2 emissions through linking pinch analysis with rigorous process models in process simulators and the MOO program. Two case studies of bi-objective optimization, for the CDU and FCC units in petroleum refineries, have been used to illustrate the optimization framework. Direct heat integration is permitted in the first case study, whilst the total site mode (indirect integration) is used in the second case. The total yield of naphtha is maximized while minimizing the total CO_2 emissions.

Despite difficulties in applying direct integration across a large site with many independent process units, the analysis of this case is useful in order to set a target for maximum energy recovery, and consequently minimum CO_2 emissions, as in the CDU/FCC integrated model studied. However, except at the lower naphtha yields, the results show no significant improvement in the target of CO_2 emissions between the direct integration case and the total site case. This means the latter case is likely to be the preferred alternative to direct integration, because of its reduced complexity of heat exchanger networks and its greater operational flexibility. However, the indirect approach does require greater capital expenditure for a larger fired heater and greater heat exchange area.

The MOO-pinch analysis framework is a rigorous method of optimizing heat-integration schemes and a powerful tool for optimizing process flow sheets for multiple economic and environmental objectives. This is the first demonstration of this technique using a total site integration approach, across two significant units in petroleum refineries.

Nomenclature

ADU	atmospheric distillation unit.
AGO	atmospheric gas oil.
APA	atmospheric distillation pump around.
APA3T	ADU PA3 return temperature (°C).
APA3F	ADU PA3 flow rate (m^3/h).
AtmT	ADU feed temperature (°C).
BFW	boiling feed water.
C%	carbon mass percent in fuel.
CC	composite curves.
CCCold	cold composite curve.
CCHot	hot composite curve.
CDU	crude distillation column.
CP	heat capacity (MW/°C).
CP_c	heat capacity of cold stream (MW/°C).
CP_h	heat capacity of hot stream (MW/°C).
CP_{cw}	heat capacity of cooling water (kJ/kg. °C).
CW	cooling water.
E_{Fact}	emission factor for a specific fuel ($kgCO_2$/kJ).

FCC	fluidized-bed catalytic cracker.
FCCT	FCC feed temperature (°C).
GCC	grand composite curve.
H	enthalpy (MW).
HEN	heat exchanger network.
HPS	high-pressure steam.
KerRQ	kerosene reboiler duty (GJ/h).
LCO	light cycle oil.
LP	linear programming.
LPS	low pressure steam.
LVGO	light vacuum gas oil.
HCO	heavy cycle oil.
HVGO	heavy vacuum gas oil.
Mc	mutation probability.
MOO	multi-objective optimization.
MPA	main fractionator pump around.
MPA3DT	main fractionator PA3 temperature drop (°C).
MPA4DT	main fractionator PA4 temperature drop (°C).
MPA3DS	main fractionator PA3 draw stage.
MPA4DS	main fractionator PA4 draw stage.
MPA3F	main fractionator PA3 flow rate (m^3/h).
MPA4F	main fractionator PA4 flow rate (m^3/h).
MPS	medium pressure steam.
NHV	net heating value of fuel (kJ/kg).
PA	pump around.
PA3	third pump around.
PA4	fourth pump around.
Pc	crossover probability.
Q_{cmin}	minimum cooling duty (MW).
Q_{hmin}	minimum heating duty (MW).
Q_{Fuel}	heat duty supplied by fuel (kJ/h).
RC	molar masses ratio of CO_2.
Ref	refrigeration.
T	temperature (°C).
T_{hot}	temperature of a hot stream (°C).
T_{cold}	temperature of a cold stream (°C).
T_{in}	inlet temperature (°C).
T_{out}	outlet temperature (°C).
T_{TFT}	theoretical flame temperature (°C).
T_o	ambient temperature (°C).
T_{Pinch}	pinch temperature (°C).
T_{stack}	stack temperature (°C).
VacT	VDU feed temperature (°C).
VBA	Visual Basic applications.
VDU	vacuum distillation unit.
VPA	vacuum distillation pump around.

VPA3T	VDU PA3 return temperature (°C).
VPA3F	VDU PA3 flow rate (m^3/h).
ΔT_{min}	minimum temperature difference (°C).
ΔH_h	enthalpy difference of hot stream (MW).
ΔH_c	enthalpy difference of cold stream (MW).
η_F	furnace efficiency.

Exercises

11.1. The GCC data of the CDU unit is given in Table 11.5 for $\Delta T_{min} = 30\,^{\circ}C$.

Table 11.5 *GCC (shifted temperature versus heat flow cascade) data for exercise 11.1.*

Shifted temperature (°C)	395	295	279	234	215	172	121	41	30
Heat flow (MW)	108	22	10	10	8	0	24	78	73

Fired heater efficiencies (η_F) can be calculated from the theoretical flame temperature $T_{TFT} = 1800\,^{\circ}C$, stack temperature, T_{stack} and ambient temperature $T_o = 25\,^{\circ}C$, according to Equation 11.6.

$$\eta_F = (T_{TFT} - T_{stack})/(T_{TFT} - T_o) \tag{11.6}$$

(a) Plot the grand composite curve for the CDU from the energy cascade provided in Table 11.5.

(b) If there is only a direct fired heater available for heating with a ΔT_{min} between the flue gas and the cold process streams of 30 °C:
   i. Calculate the fuel required to satisfy the heating requirements of the CDU.
   ii. Calculate the CO_2 emissions (using Table 11.6) in tonnes/h.
   iii. Calculate the fuel required if the stack temperature was equal to the acid dew point of 160 °C.

(c) If saturated HPS and MPS steam are both available at 260 °C and 200 °C, respectively for heating, calculate, using the GCC, the heat load that could be supplied by
   i. MPS alone;
   ii. HPS alone.

Table 11.6 *Emissions factors of utilities for exercise 1.*

Utility	Emissions factor (kg CO_2/MW.h)	Efficiency
Fuel for fired heater	193	Use equation 11.6
HPS	185	100%
MPS	160	100%

(d) Based on the emissions factor of each utility given in Table 11.6, calculate the total CO_2 emissions that occur (indirectly from the use of steam and directly from the fired heater flue gas):
   i. If MPS and HPS are both used to their maximum and flue gas makes up the remainder
   ii. If only MPS is used to its maximum and flue gas makes up the remainder

(e) Using your answers to part b(ii) and part d, discuss why there might be a conflict between minimizing the emissions from fuel from the fired heater and minimizing the total CO_2 emissions in this example.

11.2. The GCC data of the FCC unit is given in Table 11.7 for ΔT_{min} =30 °C.

Table 11.7 *GCC (temperature-heat cascade) data for exercise 2.*

Temperature (°C)	409	356	293	286	227	161	145	95	35
Heat flow (MW)	12	0	10	9	14	9	9	5	10

Calculate the maximum heat that can be recovered from hot process streams to generate HPS at 260 °C. How much cooling water (20 to 40 °C) is required to satisfy the remaining cooling requirements? $CP_{cw} = 4$ kJ/kg °C and $\Delta T_{min} = 10$ °C.

11.3. Consider the data of GCC for the CDU and FCC units given in exercises 1 and 2 respectively.

(a) Construct and plot the total site profiles.

(b) Produce targets for flue gas, HPS and MPS generated and consumed, assume $\Delta T_{min} = 30$ °C.

(c) If 8, 4 and 5 MW of respectively LPS (150 °C), MPS (200 °C) and HPS (260 °C) are required as stripping steam in the CDU and FCC units, plot steam system profiles for these two units using the total site analysis.

Appendices

A.1 Modeling of CDU and FCC

This section provides basic modeling details of the units studied in this chapter. The HYSYS file of the entire model: CDU-FCC Integrated.hsc is available in Chapter 11's folder on the web site of this book.

Among the wide range of thermodynamic property packages provided by Hysys, the Peng–Robinson (PR) equation of state is recommended for oil, gas and petrochemical applications due to its high efficiency and reliability in finding thermodynamic properties in hydrocarbon systems [40]. The PR is therefore used as the property package for the case studies presented in this chapter. More details on the PR equation of state are available in [41].

The crude oil processing capacity is set at 200 000 barrel / day, and this constitutes a blend of two types of crude oil: Arab light and Arab heavy (Safaniya). Information about crude oil assays is provided by Spiral CrudeManager® and can be found in CSV files in the folder: Chapter 11. The simulated units are the atmospheric distillation unit (ADU), vacuum distillation unit (VDU), fluidized catalytic cracker (FCC) and main fractionator. Design data for simulating these units are given in Tables 11.A1 to 11.A4.

Table 11.A1 *Design data for simulating ADU.*

No of trays	29[a]
Feed location	28
Top-stage pressure	198 kPa
Bottom-stage pressure	225 kPa
Overflash	1 vol%
Naphtha 95% cut point	190 °C
Kerosene withdraw stage	9
Kerosene 95% cut point	271 °C
Diesel withdraw stage	17
Diesel 95% cut point	327 °C
Diesel stripping stages	3
AGO withdraw stage	22
AGO stripping stages	3
APA1 (withdraw–return) stage	2–1
APA1 flow rate	400 m^3/h
APA2 (withdraw –return) stage	17–16
APA2 flow rate	400 m^3/h
APA3 (withdraw –return) stage	22–21
APA3 flow rate	283 m^3/h

[a]Tray numbers are excluding the condenser tray and counted from the top of the column.

Table 11.A2 *Design data for simulating VDU.*

No of trays	9[a]
Feed location	8
Top stage pressure	11 kPa
Bottom stage pressure	13 kPa
LVGO withdraw stage	2
LVGO 95% cut point	430
HVGO withdraw stage	6
HVGO 95% cut point	500
VPA1 (withdraw–return) stage	2–1
VPA1 flow rate	300 m^3/h
VPA2 (withdraw–return) stage	6–5
VPA2 flow rate	200 m^3/h
VPA3 (withdraw–return) stage	9–8
VPA3 flow rate	198.3 m^3/h

[a]Tray numbers are excluding the condenser tray and counted from the top of the column.

Table 11.A3 *Design data for simulating FCC.*

Feed type	Vacuum gas oil
Reactor pressure	430 kPa
Regenerator–reactor pressure difference	30 kPa
Catalyst inventory	90 720 kg
Fresh catalyst make up rate	53.34 kg/h
Stripping steam temperature	200 °C
Stripping steam pressure	1000 kPa
Stripping steam ratio to catalyst circulation rate (×1000)	3

Table 11.A4 *Design data for simulating main fractionator.*

No. of trays	13[a]
Feed location	13
Top stage pressure	300 kPa
Bottom stage pressure	320 kPa
Condenser temperature	50 °C
Naphtha 95% cut point	220 °C
LCO withdraw stage	4
LCO stripping stages	3
HCO withdraw stage	8
HCO stripping stages	3
AGO withdraw stage	22
AGO stripping stages	3
MPA1 (withdraw–return) stage	2–1
MPA1 flow rate	100 m^3/h
MPA2 (withdraw –return) stage	6–5
MPA2 flow rate	100 m^3/h

[a]Tray numbers are excluding the condenser tray and counted from the top of the column.

A.2 Preliminary Results with Different Values for NSGA-II Parameters

Figures 11.A1 to 11.A2 show the preliminary experimentation that was undertaken to obtain suitable values of the computational parameters in the NSGA-II.

A.3 Pinch Analysis Techniques

This appendix illustrates the construction of CC, GCC, and total site profiles used in this chapter. A typical problem of two simple processes is considered. Data for the process streams of the two processes are shown in Table 11.A5; assume ΔT_{min} is 30 °C. The procedure of applying pinch analysis is divided into three main steps: CC, GCC, and total site profiles.

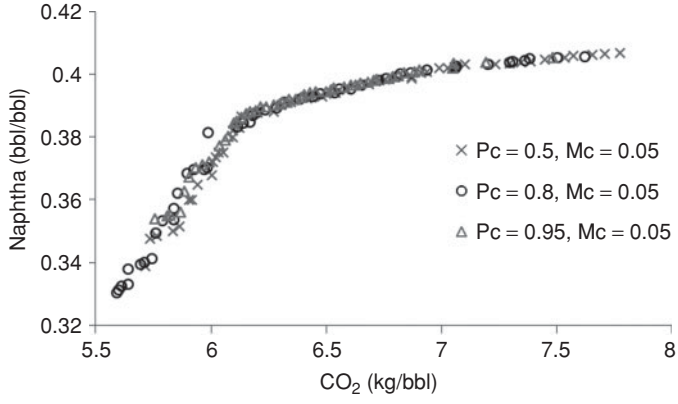

Figure 11.A1 *Effect of crossover probability on the results after 50 generations.*

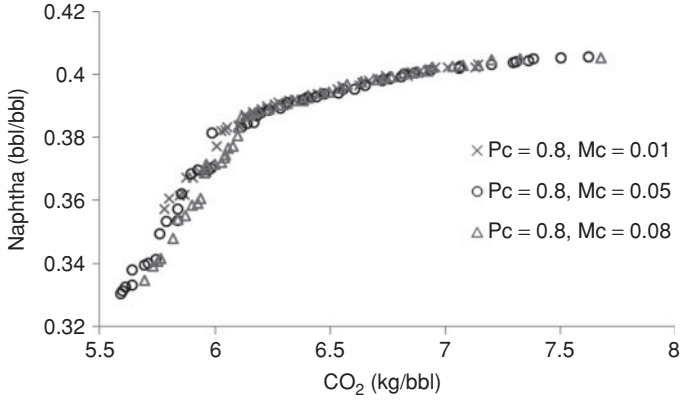

Figure 11.A2 *Effect of mutation probability on the results after 50 generations.*

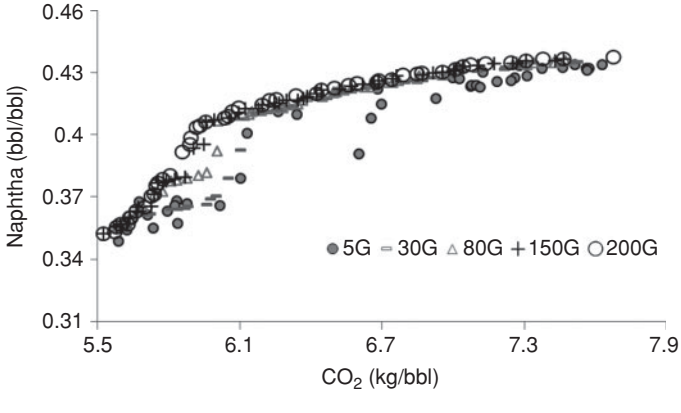

Figure 11.A3 *Results at different maximum number of generations, for case study-1.*

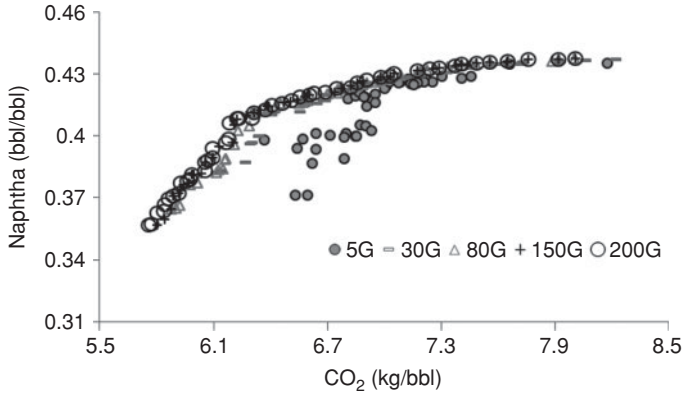

Figure 11.A4 *Results at different maximum number of generations, for case study-2.*

A.3.1 Composite Curves (CC)

1. Extract the data for all the process streams, and categorize them into cold and hot streams as shown in Table 11.A6; cold streams require heating whereas hot streams require cooling.
2. Assume ΔT_{min} is 30 °C. Shift temperatures of the cold streams by $+\frac{1}{2}\Delta T_{min}$ ($= +15$ °C) and temperatures of the hot streams by $-\frac{1}{2}\Delta T_{min}$ ($= -15$ °C).
3. Calculate CP for each stream using the following equation:

$$CP = \Delta H/(T_{out} - T_{in}) \tag{11.A1}$$

   Note that hot streams have negative CP values and cold streams have positive CP values.
4. Classify and break down all hot and cold streams into temperature intervals as shown in Table 11.A7 for Process 1.
5. Calculate the sum of the heat capacities of the hot streams (CP_h) and the cold streams (CP_c) in each of the temperature intervals, and then calculate heat flows, ΔH_h and ΔH_c, using the rearranged form of Equation 11.A1.

Table 11.A5 *Processes and their streams data.*

No	Stream	T_{in} (°C)	T_{out} (°C)	ΔH (MW)
Process 1				
1	P1-1	100	400	10
2	P1-2	230	60	5
3	P1-3	350	100	50
Process 2				
1	P2-1	20	300	50
2	P2-2	60	100	3
3	P2-3	200	150	15
4	P2-4	150	100	25

Table 11.A6 *Process stream data.*

No	Status	Stream	T_{in} (°C)	T_{out} (°C)	T_{in*} (°C)	T_{out}[a] (°C)	ΔH (MW)	CP (MW/°C)
Process 1								
1	Cold	P1–1	100	400	115	415	10	0.03
2	Hot	P1–2	230	60	215	45	5	−0.03
3	Hot	P1–3	350	100	335	85	50	−0.20
Process 2								
1	Cold	P2–1	20	300	35	315	50	0.18
2	Cold	P2–2	60	100	75	115	3	0.08
3	Hot	P2–3	200	150	185	135	15	−0.30
4	Hot	P2–4	150	100	135	85	25	−0.50

[a]Shifted temperature.

6. Calculate the cumulated ΔH values to find ΣΔH for all hot/cold streams (see columns 9 and 11 in Table 11.A7).
7. $\Sigma\Delta H_h$ and $\Sigma\Delta H_c$ shown in columns 9 and 11 respectively in Table 11.A7 are plotted against the shifted temperatures (column 1 in Table 11.A7) to generate Figure 11.A5. ΣΔHc values (dashed curve in Figure 11.A5) are shifted by the maximum gap between ΣΔHh and ΣΔHc as shown in Table 11.A7 (CCCold values) and Figure 11.A5 (solid curve).
8. The hot and cold composite curves can be created by plotting ΣΔH values (CCHot and CCCold) from Table 11.A7 versus the corresponding temperatures after shifting the temperatures back to real temperatures, as shown in Figure 11.A6 for Process 1.
9. Steps 4 to 8 are repeated for Process 2 as shown in Tables 11.A8 and 11.A10 and Figures 11.A7 and 11.A9.

Table 11.A7 *Data for composite curves of Process 1.*

		CP												
T (°C) (shifted)	ΔT	P1−1	P1−2	P1−3	ΣCP_h	ΣCP_c	$\Delta H_h = \Sigma CP_h \times \Delta T$	$\Sigma\Delta H_h$	$\Delta H_c = \Sigma CP_c \times \Delta T$	$\Sigma\Delta H_c$	T_{hot}(unshifted)	CCHot	T_{cold}(unshifted)	CCCold
45	40	0	−0.03	0	0.03	0	1.18	0	0	0	60	0	30	47.67
85	30	0	−0.03	−0.2	0.23	0	6.88	1.18	0	0	100	1.18	70	47.67
115	100	0.03	−0.03	−0.2	0.23	0.03	22.94	8.06	3.33	0	130	8.06	100	47.67
215	120	0.03	0	−0.2	0.2	0.03	24	31	4	3.33	230	31	200	51
335	80	0.03	0	0	0	0.03	0	55	2.67	7.33	350	55	320	55
415								55		10	430	55	400	57.67

Table 11.A8 *Data for composite curves of Process 2.*

		CP													
T (°C) (shifted)	ΔT	P2−3	P2−4	P2−2	P2−1	ΣCP_h	ΣCP_c	$\Delta H_h = \Sigma CP_h \times \Delta T$	$\Sigma \Delta H_h$	$\Delta H_c = \Sigma CP_c \times \Delta T$	$\Sigma \Delta H_c$	T_{hot}(unshifted)	CCHot	T_{cold}(unshifted)	CCCold
35	40	0	0	0	0.18	0	0.18	0	0	7.14	0	50	0	20	10.21
75	10	0	0	0.08	0.18	0	0.25	0	0	2.54	7.14	90	0	60	17.36
85	30	0	−0.5	0.08	0.18	0.5	0.25	15	0	7.61	9.68	100	0	70	19.89
115	20	0	−0.5	0	0.18	0.5	0.18	10	15	3.57	17.29	130	15	100	27.5
135	50	−0.3	0	0	0.18	0.3	0.18	15	25	8.93	20.86	150	25	120	31.07
185	130	0	0	0	0.18	0	0.18	0	40	23.21	29.79	200	40	170	40
315									40		53	330	40	300	63.21

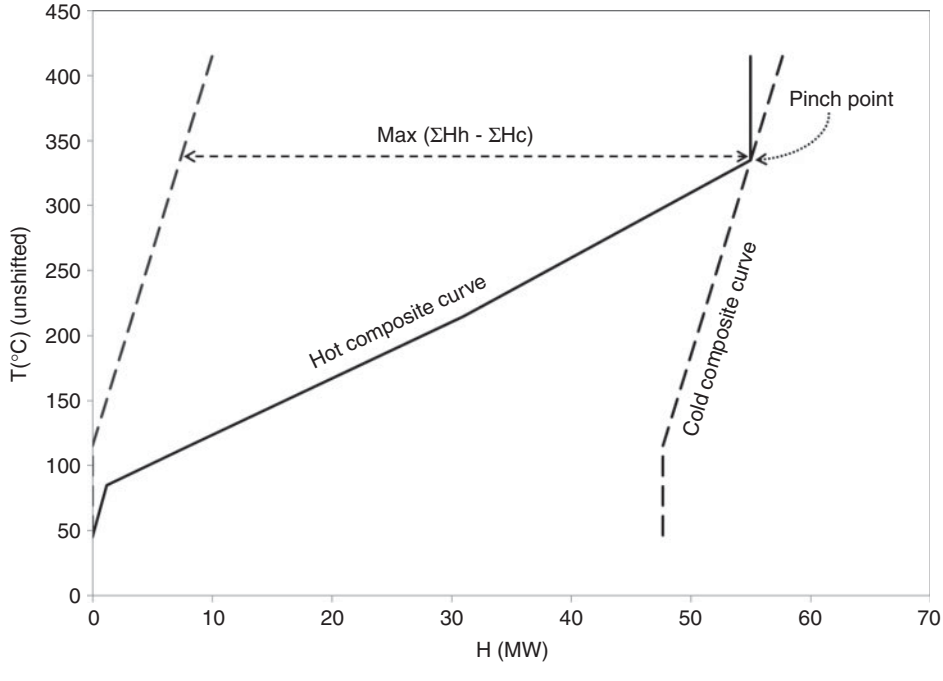

Figure 11.A5 *Construction of CC of Process 1.*

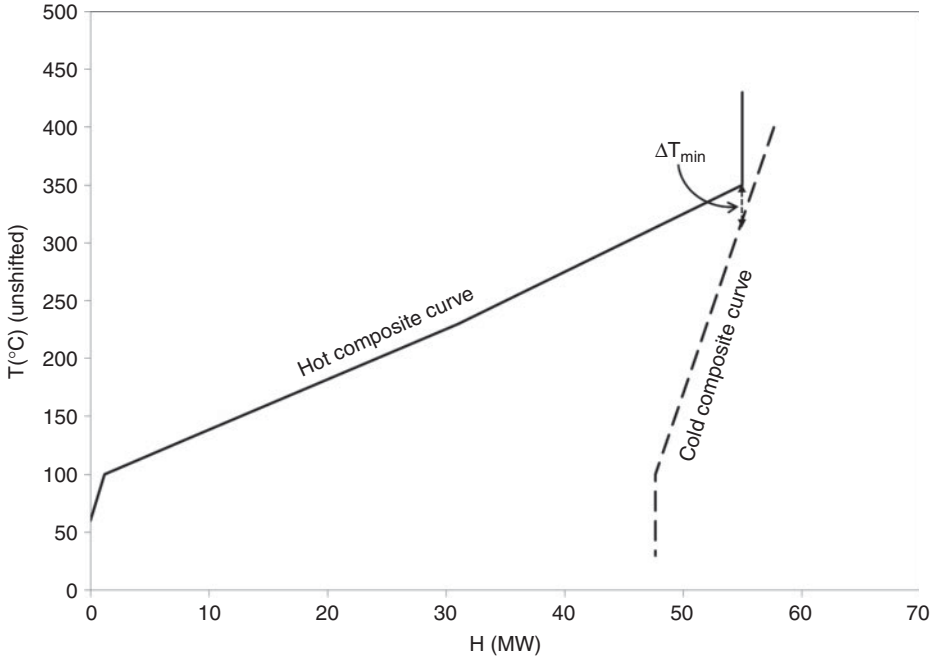

Figure 11.A6 *Hot and cold composite curves of Process 1.*

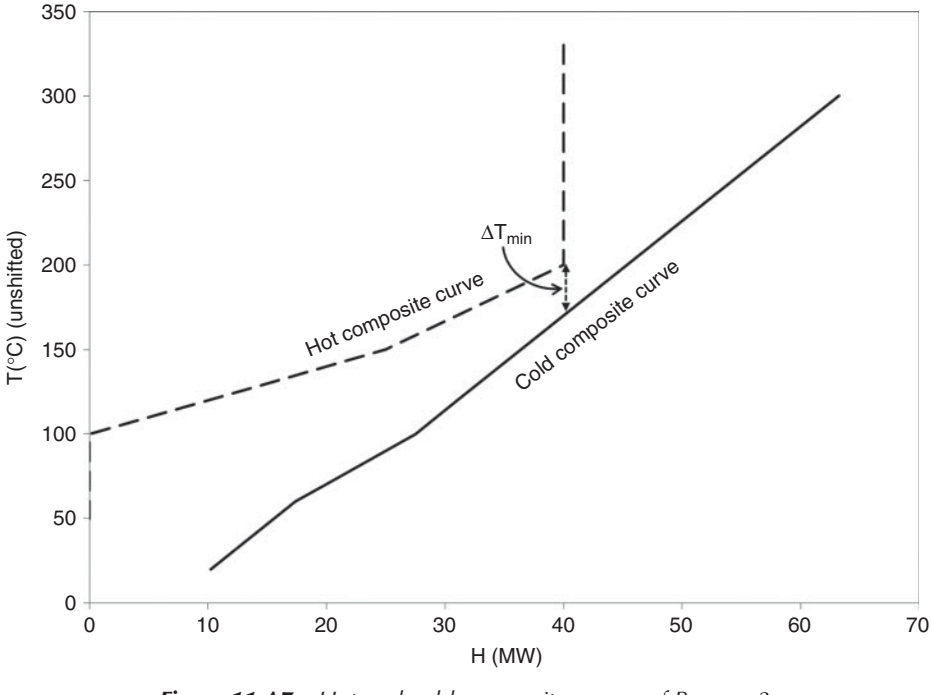

Figure 11.A7 *Hot and cold composite curves of Process 2.*

Table 11.A9 *Data for GCC of Process 1.*

T (°C) (shifted)	ΔT	CP P1−1	CP P1−2	CP P1−3	ΣCP_h	ΣCP_c	$\Delta Cp = \Sigma CP_c - \Sigma CP_h$	$\Delta H = \Delta Cp \times \Delta T$	Heat flow	Positive heat flow
45	40	0	−0.03	0	0.03	0	−0.03	−1.18	45	47.67
85	30	0	−0.03	−0.2	0.23	0	−0.23	−6.88	43.82	46.49
115	100	0.03	−0.03	−0.2	0.23	0.03	−0.2	−19.61	36.94	39.61
215	120	0.03	0	−0.2	0.2	0.03	−0.17	−20	17.33	20
335	80	0.03	0	0	0	0.03	0.03	2.67	−2.67	0
415									0	2.67

A.3.2 Grand Composite Curve (GCC)

1. Calculate net Cp for each temperature interval using the equation:

$$\Delta Cp = \sum CP_c - \sum CP_h \tag{11.A2}$$

2. Calculate ΔH for each temperature interval using the modified form of Equation 11.A1. See the values for Process 1 in Table 11.A9.
3. Calculate the accumulated ΔH values to find heat flow for all temperature intervals.
4. In order to get positive heat flow, add the absolute value of minimum negative heat flow (−2.67 in Table 11.A9) to all values of heat flow.
5. The GCC can be created by plotting values of positive heat flow versus the corresponding temperatures (shifted) from the first and last column of Table 11.A9, as shown in Figure 11.A8.
6. For Process 2, data for GCC are in Table 11.A10, and GCC is shown in Figure 11.A9.

A.3.3 Total Site Profiles

1. Split the GCC of each process into two parts, below and above pinch points to identify the residual heat sources and heat sinks of each process (Figure 11.A10).

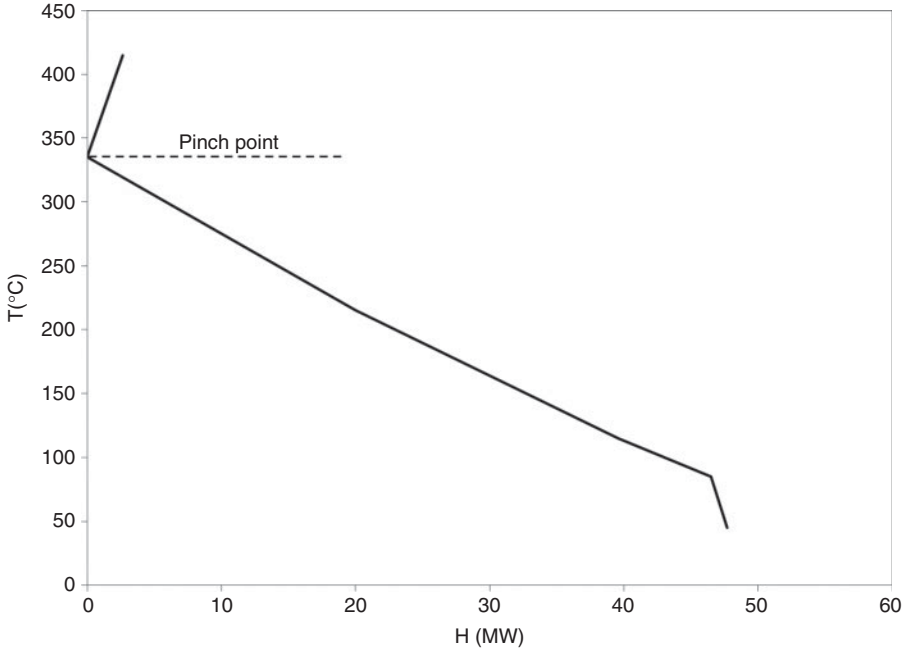

Figure 11.A8 *GCC of Process 1.*

Table 11.A10 *Data for GCC of Process 2.*

		CP									
T (°C) (shifted)	ΔT	P2−3	P2−4	P2−2	P2−1	ΣCP_h	ΣCP_c	$\Delta Cp = \Sigma CP_c - \Sigma CP_h$	$\Delta H = \Delta Cp \times \Delta T$	Heat flow	Positive heat flow
35	40	0	0	0	0.18	0	0.18	0.18	7.14	−13	10.21
75	10	0	0	0.08	0.18	0	0.25	0.25	2.54	−5.86	17.36
85	30	0	−0.5	0.08	0.18	0.5	0.25	−0.25	−7.39	−3.32	19.89
115	20	0	−0.5	0	0.18	0.5	0.18	−0.32	−6.43	−10.71	12.5
135	50	−0.3	0	0	0.18	0.3	0.18	−0.12	−6.07	−17.14	6.07
185	130	0	0	0	0.18	0	0.18	0.18	23.21	−23.21	0
315										0	23.21

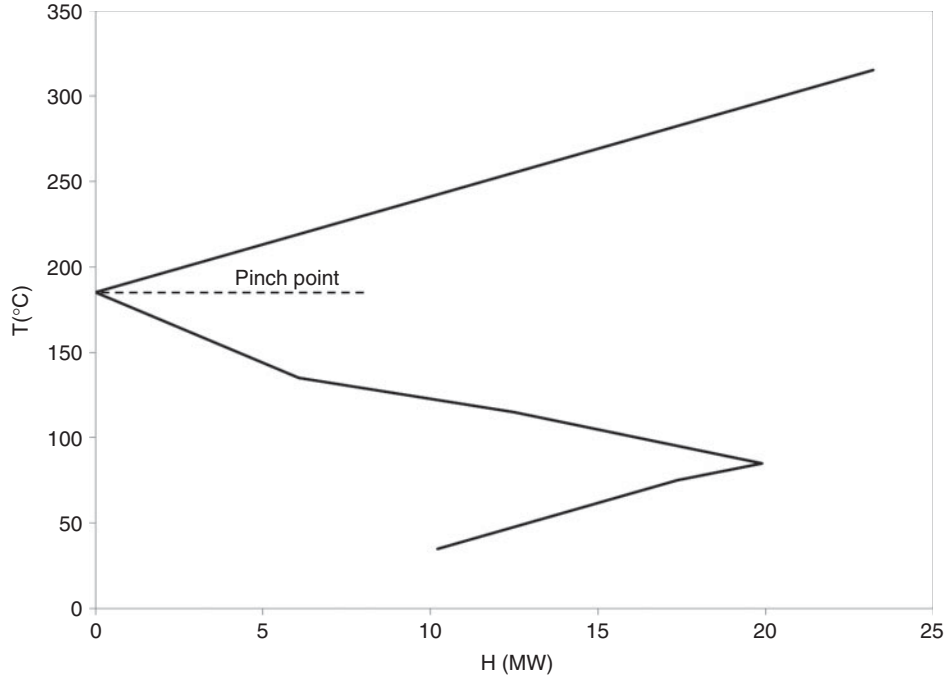

Figure 11.A9 *GCC of Process 2.*

2. Exclude the process-to-process heat recovery (pockets) from each individual GCC as shown in the GCC of Process 2 (Figure 11.A10).
3. Classify, break down and extend temperature intervals of all processes below and above pinch point, as shown in Tables 11.A11 and 11.A12.
4. Use interpolation to fill missing values (if any) of enthalpies at new temperature intervals.
5. Calculate the total enthalpy (total site) for each temperature interval by combining the enthalpies from both processes.
6. Shift temperatures back to real temperatures by adding $^1/_2\ \Delta T_{min}$ in case of total site heat sink and subtract $^1/_2\ \Delta T_{min}$ in case of total site heat source.
7. Then, the overall surplus heat and the heat deficit for both processes can be determined using the total site profiles. The amount of steam that can be generated/used on the total site via different steam mains can be found from the total site composite curves, as shown in Figure 11.A11.

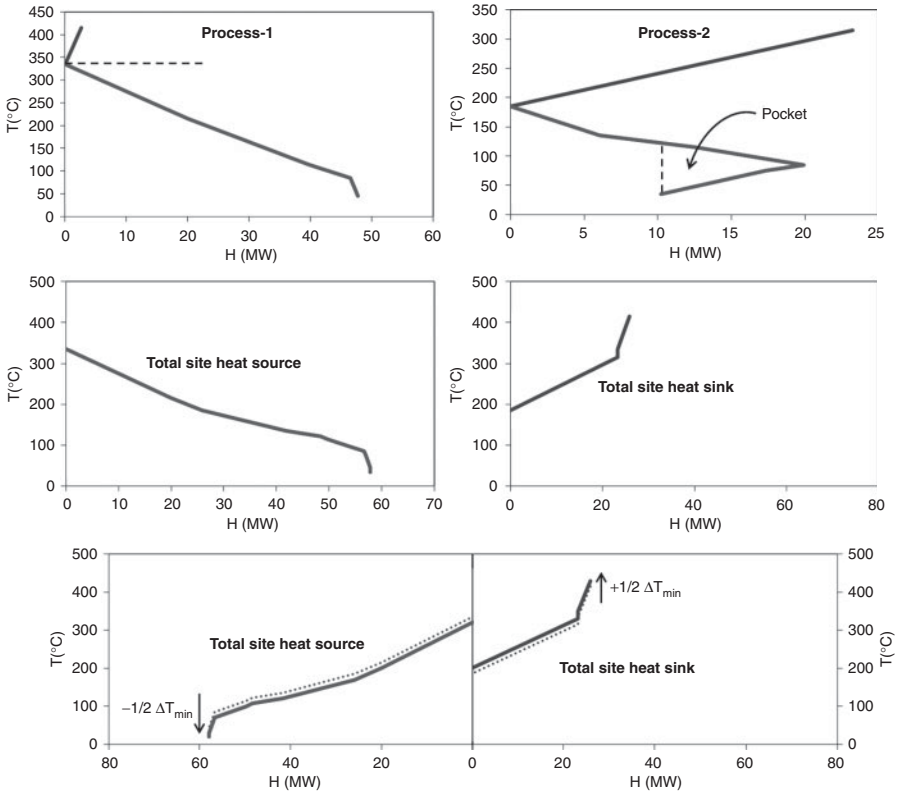

Figure 11.A10 *Construction of total site profiles.*

Table 11.A11 *Data for total site heat sink.*

GCC – Process 1		GCC – Process 2		T intervals above pinch (shifted)	H			Total site heat sink
T	H	T	H		Process 1	Process 2	Total H	T (real)
415	2.67	315	23.21	415	2.67	23.21	25.88	430
335	0	185	0	335	0	23.21	23.21	350
215	20	135	6.07	315	0	23.21	23.21	330
115	39.61	115	12.5	185	0	0	0	200
85	46.49	85	19.89					
45	47.67	75	17.36					
		35	10.21					

Table 11.A12 *Data for total site heat source.*

GCC – Process 1		GCC – Process 2		T intervals below pinch (shifted)	H		Total site heat source	
T	H	T	H		Process 1	Process 2	Total H	T (real)
415	2.67	315	23.21	35	47.67	10.21	57.88	20
335	0	185	0	45	47.67	10.21	57.88	30
215	20	135	6.07	75	46.78	10.21	57	60
115	39.61	115	12.5	85	46.49	10.21	56.7	70
85	46.49	85	19.89	85	46.49	10.21	56.7	70
45	47.67	75	17.36	115	39.61	10.21	49.82	100
		35	10.21	115	39.61	10.21	49.82	100
				122	38.21	10.21	48.43	107
				135	35.69	6.07	41.76	120
				185	25.88	0	25.88	170
				215	20	0	20	200
				335	0	0	0	320

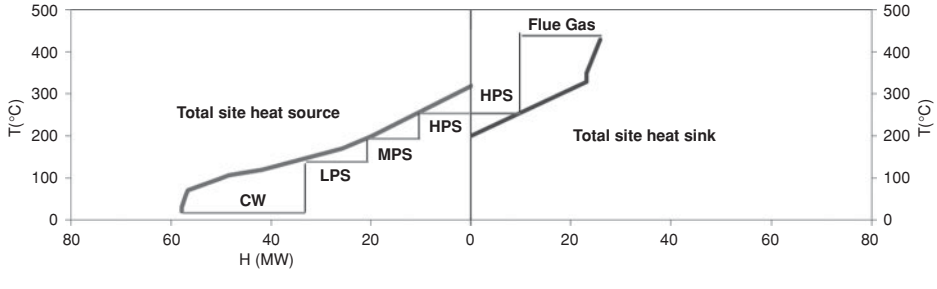

Figure 11.A11 *Total site profiles along with possible steam use/generation.*

References

[1] D. Babusiaux, Allocation of the CO2 and pollutant emissions of a refinery to petroleum finished product. Oil and Gas Science and Technology, 6, 685–692 (2003).

[2] D. Babusiaux, and A. Pierru, Modelling and allocation of CO2 emissions in a multiproduct industry: The case of oil refining. Applied Energy, 84, 828–841 (2007).

[3] A. Pierru, Allocating the CO_2 emissions of an oil refinery with Aumann–Shapley prices. Energy Economics, 29, 563–577 (2007).

[4] A.N. Tehrani, Allocation of CO2 emissions in petroleum refineries to petroleum joint products: A linear programming model for practical application. Energy Economics, 29, 974–997 (2007).

[5] A.N. Tehrani, Allocation of CO2 emissions in joint product industries via linear programming: A refinery example. Oil and Gas Science and Technology, 5, 653–662 (2007).

[6] A. Szklo, and R. Schaeffer, Fuel specification, energy consumption and CO_2 emission in oil refineries. Energy, 32, 1075–1092 (2007).

[7] M.S. Ba-Shammakh, An optimization approach for integrating planning and CO2 mitigation in the power and refinery sectors. Ph.D. thesis (2007), University of Waterloo.

[8] T. Greek, Role of carbon capture in CO2 management. Petroleum Technology Quarterly. Spring, 63–69 (2004).

[9] I. Moore, Reducing CO_2 emissions. Petroleum Technology Quarterly, Q2, 1–6 (2005).

[10] K. Ritter, S. Nordrum, T. Shires and M. Levon, Ensuring consistent greenhouse gas emissions estimates. Chemical Engineering Processes. September, 30–37 (2005).

[11] J.N. Mertens, K. Minks and R.M. Spoor, Refinery CO_2 challenges, Part III: For the prediction of CO_2 emissions from a refinery, simple correlations are not always sufficient. A rigorous simulation tool that includes fractionation and reactor models can help to obtain a correct prediction of the total emissions. Petroleum Technology Quarterly, July, 113–121 (2006).

[12] V. Bruna, J. Hart and A. Rudman, Refinery CO_2 challenges: part IV, Reducing CO_2 emissions with a strategic energy-improvement programmme. Petroleum Technology Quarterly, Q4 (2006).

[13] R.M. Spoor, Refinery CO_2 challenges, Part I: measuring, reporting and reduction of CO_2 emissions, Petroleum Technology Quarterly, Q1, 1–5 (2006).

[14] K. Holmgren and C. Sternhufvud, CO_2-emission reduction costs for petroleum refineries in Sweden. Journal of Cleaner Production, 16, 385–394 (2008).

[15] M. Stockle, D. Carter and L. Jounes, Optimising refinery CO2 emissions. Petroleum Technology Quarterly, Q1, 123–130 (2008).

[16] S. Ratan and R. Uffelen, Curtailing refinery CO_2 through H_2 plant. Petroleum Technology Quarterly, Gas, 19–23 (2008).

[17] J. Mertens, and J. Skelland, Rising to the CO_2 challenge, Part 3: CO_2 emissions reduction options in refineries, Hydrocarbon Engineering, March (2010).

[18] D. Carter, Improving refinery margins and reducing CO_2, Green Forum, Dubrovnik 17 June (2011).

[19] B.A. Al-Riyami, J. Klemes, and S. Perry, Heat integration retrofit analysis of a heat exchanger network of a fluid catalytic cracking plant, Applied Thermal Engineering, 21, 1449–1487 (2001).
[20] V.R. Dhole, and B. Linnhoff, Total site targets for fuel, co-generation, emissions, and cooling, Computational and Chemical Engineering, 17, S101–S109 (1993).
[21] B. Linnhoff and A.R. Eastwood, Overall site optimization by pinch technology, Chemical Engineering Research and Design, 65, S138–S144 (1987).
[22] M. Ebrahim and A. Kawari, Pinch technology: an efficient tool for chemical plant energy and capital-cost saving, Applied Energy, 65, 45–49 (2000).
[23] M.M. Shanazari, F. Shahraki and M. Khorram, Retrofit of crude distillation unit using process simulation and process integration, Proceedings of Chemeca, Melbourne, Australia (2007).
[24] J. Klemes, V.R. Dhole, K. Raissi, S.J. Perry and L. Puigjanerl, Targeting and design methodology for reduction of fuel, power and CO, on total sites, Applied Thermal Engineering, 17, 993–1003 (1997).
[25] K. Liebmann, V.R. Dhole, M. Jobson, Integrated design of a conventional crude oil distillation tower using pinch analysis. Chemical Engineering Research and Design, 76(3), 335–347 (1998).
[26] R.N. Watkins, Petroleum Refinery Distillation, 2nd edition, Gulf Publishing Company, Houston, Texas (1979).
[27] M.A. Al-Mayyahi, A.F.A. Hoadley, N.E. Smith and G.P. Rangaiah, Investigating the trade-off between operating revenue and CO_2 emissions from crude oil distillation using a blend of two crudes, Fuel, 90(12), 3577–3585 (2011).
[28] M. Gadalla, Z. Olujic, M. Jobson and R. Smith, Estimation and reduction of CO_2 emissions from crude oil distillation units, Energy, 31(13), 2398–2408 (2006).
[29] E. Worrell and C. Galitsky, Energy efficiency improvement and cost saving opportunities for petroleum refineries, Environmental Energy Technologies Division, Berkeley, USA, February (2005).
[30] M.A. Al-Mayyahi, A.F.A. Hoadley, N.E. Smith and G.P. Rangaiah, Multi-objective optimization of a fluidized bed catalytic cracker unit to minimize CO_2 emissions, Proceedings of Chemeca, Sydney, Australia (2011).
[31] D. Boland, B. Linnhoff, The preliminary design of networks for heat exchange by systematic methods, Chemical Engineering, 222, April (1979).
[32] R. Smith, (2005) Chemical Process Design and Integration, John Wiley & Sons, Ltd.
[33] I.C. Kemp, (2006) Pinch Analysis and Process Integration: A User Guide on Process Integration for the Efficient Use of Energy, 2nd edition, Butterworth-Heinemann.
[34] B. Linnhoff and V.R. Dhole, Targeting for CO_2 emissions for total sites, Chemical Engineering Technology, 16, 256–259 (1993).
[35] G.P. Rangaiah, (2009) Advances in Process Systems Engineering: Multi-Objective Optimization, Techniques and Applications in Chemical Engineering, World Scientific Publishing.
[36] S. Sharama, G.P. Rangaiah and K.S. Cheah, Multi-objective optimization using MSExcel with an application to design of a falling-film evaporator system, Food and Bioproducts Processing, 90, 123–134 (2012).
[37] K.A. Golonka and D.J. Brennan, Application of life cycle assesment to process selection for pollutant treatment: A case study of sulfur dioxide emissions from Australia

metallurgical smelters. Transactions of the Institution of Chemical Engineers, 74(B), May 105–119 (1996).
[38] M.J. Bagajewicz and S. Ji, Rigorous procedure for the design of conventional atmospheric crude fractionation units. Part I: Targeting, Industrial and Engineering Chemistry Research 40(2), 617–626 (2011).
[39] D. Dave and N. Zhang, Multiobjective optimization of fluid catalytic cracker unit using genetic algorithms. Computer Aided Chemical Engineering, 14, 623–628(2003).
[40] Hyprotech Manuals, HYSYS 2.4 (Update), Appendix A—Property Methods and Calculations, AEA Technology, 2001 Hyprotech Ltd., pp. A1–69.
[41] D.Y. Peng and D.B. Robinson, A new two constant equation of state, Industrial and Engineering Chemistry Fundamentals, 15, 59–64 (1976).